Title: Myostatin gene deletion alters gut microbiota stimulating fast-twitch glycolytic muscle growth

Short title: MSTN KO–gut microbiota promote muscle growth

Authors

Zhao-Bo Luo[2†], Shengzhong Han[2†], Xi-Jun Yin[2,3†], Hongye Liu[2], Junxia Wang[2], Meifu Xuan[2], Chunyun Hao[4], Danqi Wang[4], Yize Liu[1], Shuangyan Chang[2], Dongxu Li[4], Kai Gao[2], Huiling Li[3], Biaohu Quan[2,3], Lin-Hu Quan[1]*, and Jin-Dan Kang[2,3]*

Affiliations

[1]Key Laboratory of Natural Medicines of the Changbai Mountain, Ministry of Education, College of Pharmacy, Yanbian University; Yanji, 133002, China.

[2]Department of Animal Science, College of Agricultural, Yanbian University; Yanji, 133002, China.

[3]Jilin Provincial Key Laboratory of Transgenic Animal and Embryo Engineering, Yanbian University; Yanji, 133002, China.

[4]College of Integration Science, Yanbian University; Yanji, 133002, China.

[†]These authors contributed equally.

[*]Correspondence:

Lin-Hu Quan, Key Laboratory of Natural Medicines of the Changbai Mountain, Ministry of Education, College of Pharmacy, Yanbian University, Yanji, 133002, China, Tel./Fax: +86-433-2436452, Email address: lhquan@ybu.edu.cn.

Jin-Dan Kang, Department of Animal Science, College of Agricultural, Yanbian University; Yanji, 133002, China, Tel./Fax: +86-433-2435623, E-mail address: jdkang@ybu.edu.cn

Abstract The host genome may influence the composition of the intestinal microbiota, and intestinal microbiota performs an important role in muscle growth and development. Here, we showed that Myostatin (MSTN), a key factor for muscle growth, deletion alters muscularis, plica, and intestinal barrier in pigs. Mice transplanted with *MSTN*$^{-/-}$ pig intestinal flora showed increase in the cross-sectional area of myofibers and fast-twitch glycolytic muscle mass. The microbes responsible for the production of short chain fatty acids (SCFAs) were enriched in both *MSTN*$^{-/-}$ pigs and recipient mice, and SCFAs levels were elevated in the colon contents. We demonstrated that valeric acid can stimulate type IIb myofiber growth by activation of the Akt/mTOR pathway via GPR43 and improve muscle atrophy induced by dexamethasone. This is the first study to identify the *MSTN* gene-gut microbiota-SCFA axis and its regulatory role in fast-twitch glycolytic muscle growth.

Introduction

The decline in muscle mass is a considerable health problem that deteriorates the quality of life and increases disease occurrence and mortality (Newman et al., 2006; Srikanthan et al., 2014). For instance, a decrease in muscle mass contributes to the onset of various diseases, such as sarcopenia, obesity, diabetes, and cancer. Myostatin (MSTN), a transforming growth factor β family member, is among the major regulators of skeletal muscle growth and development (Chen et al., 2021). Substantial muscle hypertrophy was observed in *MSTN* mutant animals and humans (McPherron et al., 1997; Ceccobelli et al., 2022; McPherron and Lee, 1997; Kambadur et al., 1997; Mosher et al., 2007; Kang et al., 2017; Schuelke et al., 2004). Recently various MSTN inhibitors, including monoclonal antibodies, have been tested in clinical trials to treat muscle disorders, such as sarcopenia and cancer-associated cachexia (Kim et al., 2021; Cho et al., 2022). Notably, *MSTN* is not only expressed in skeletal muscles, but also in smooth muscles including the intestine, to participate in various metabolic processes (Sundaresan et al., 2008; Verzola et al., 2017; Esposito et al., 2020; Kovanecz et al., 2017). Previous studies have shown that *MSTN* mutation can alter the composition of intestinal flora in pigs (Pei et al., 2021). However, the interaction between the gut microbiota reshaped by *MSTN* deletion and the host is unclear.

Genetic variation can reshape the structure of the gut microbiota. Mutation in human *SLC30A2* leads to reduced intestinal zinc transport and increased *Clostridiales* and *Bacteroidales* abundance, causing mucosal inflammation and intestinal dysfunction (Kelleher et al., 2022). Moreover, the gut *GLUT1* gene deletion altered the abundances of *Barnesiella intestinis* and *Faecalibaculum rodentium*, promoted fat accumulation, and impaired sugar

tolerance (He et al., 2022). These results suggest that host genes can influence the gut microbiota, thereby regulating physiological processes. Intestinal structural changes, such as in intestinal length, epithelial thickness, and surface area by surgery, could affect intestinal function and microbial composition (Seganfredo et al., 2017; Nicoletti et al., 2017; Agus et al., 2018). Barrier defects were accompanied by major changes in the fecal microbiota and a significantly decreased abundance of *Akkermansia muciniphila*, increaseing the vulnerability to gastrointestinal disorders (Sovran et al., 2019).

The intestinal microbiota plays a crucial role in muscle growth and development. For example, urease gene-rich microbes, *Alistipes* and *Veillonella* respectively maintain muscle mass in hibernating animals by promoting urea nitrogen salvage (Regan et al., 2022) and metabolize lactic acid to provide energy for skeletal muscles for long periods of exercise and increase endurance in runners (Scheiman et al., 2019). Short chain fatty acids (SCFAs) are gut microbiota-derived metabolites that are involved in maintaining the integrity of the intestinal mucosa, improving glucose and lipid metabolism, controlling energy expenditure, and regulating the immune system and inflammatory responses (Agus et al., 2021; Besten et al., 2013). SCFAs are absorbed in gut lumen and mediate host metabolic responses in various organs, including skeletal muscle (Frampton et al., 2020). SCFAs play a vital role in skeletal muscle mass maintenance (Lv et al., 2021; Chen et al., 2022), and are involved in the regulation of lipid and glucose metabolism primarily through G protein-coupled receptors (GPRs), such as GPR41, GPR43, and GPR109 (Stoddart et al., 2008; Hul et al., 2019).

Skeletal myofibers exhibit remarkable diversity and plasticity in energy metabolism and contractile functions. Slow-twitch muscles are rich in mitochondria and have high oxidative

capacity, whereas fast-twitch muscles generate ATP primarily through glycolysis (Schiaffino et al., 2011; Bassel-Duby et al., 2006). Aging and muscle atrophy result in a gradual decline in muscle mass and strength accompanied by a higher proportion of type I myofibers, leading to muscle weakness due to the preferential loss and atrophy of fast-twitch glycolytic type IIb myofibers (Akasaki et al., 2014; Haber et al., 1992; Faulkner et al., 2007; Kirkendall et al., 1998). Type IIb myofibers are larger in size and more glycolytic and generate high contractile force, but have poorer resistance to fatigue than type I myofibers (Schiaffino et al., 2011). The activation of Akt/mTOR was confirmed to promote the transition from oxidized to glycolytic myofiber types by elevating the levels of glycolytic proteins HK2, PFK1, and PKM2 (Meng et al., 2013; Izumiya et al., 2008; Verbrugge et al., 2020).

MSTN can affect the growth and function of skeletal muscles. This study aimed to investigate whether the intestinal flora remodeled by *MSTN* deletion is involved in the regulation of skeletal muscle growth. Because pigs are highly similar to humans in many aspects such as physiology, disease progression and organ structure (Swindle et al., 2012), we used $MSTN^{-/-}$ pigs to investigate the effects of *MSTN* deletion on intestinal structure and the relationship between intestinal microbiota and skeletal muscle growth and function and to explore the underlying mechanisms involved in the regulation of muscle growth by the *MSTN* gene–gut microbiota–skeletal muscle axis.

Results

MSTN deletion stimulates muscle hypertrophy and alters intestinal structure and composition of gut microbiota in pigs

We used *MSTN*$^{-/-}$ pigs with 2 and 4 bp deletions in the two alleles of the *MSTN* gene (Figure 1-figure supplement 1A). They were generated using the TALEN genome editing technique (Kang et al., 2017). We found that those pigs had higher skeletal muscle mass and myofiber CSA but lost MSTN expression and reduced phosphorylation of smad2/3 in skeletal muscles (Figure 1A-C). The protein expression of myosin heavy chain (MyHC) type IIb, MyoD and glycolytic enzymes HK2, PFK1 and PKM2 were significantly increased in skeletal muscle (Figure 1C, D). The expression of MSTN was not detected in intestine, whereas that of smooth muscle proteins α-SMA and calponin-1 was increased (Figure 1E). We also observed an increase in muscularis thickness and plica length of intestinal and upregulated expression of tight junction-related genes *ZO-1* and *Occludin* (Figure 1F, G). These findings indicate that *MSTN* knockout leads to changes in intestinal structure.

Because host genotypes and phenotypes in various mammals interact with the gut microbiota (Kreznar et al., 2017), we speculated that *MSTN* deletion could affect the composition of the gut microbiota by altering intestinal structure. Thus, fecal samples from *MSTN*$^{-/-}$ and wild-type (WT) pigs were examined to determine the diversity and abundance of gut microbiota using 16s rRNA-based microbiota analysis. The alpha-diversity values showed that the ACE in *MSTN*$^{-/-}$ pigs are significantly lower than that in WT pigs; however, Chao 1, Shannon, and Simpson indexes were no significant difference (Figure 1-figure supplement 1B-E). These results suggest that *MSTN* deficiency can lead to a decrease in the abundance of intestinal flora. The composition structure of the gut microbiota, as analyzed by PCA, showed that the two groups can be clearly differentiated (Figure 1H). LEfSe analysis confirmed a significant difference at the genus level in *Romboutsia* (Figure 1I). In addition,

153 *Treponema*, *Romboutsia*, and *Turicibacter* were significantly increased at the genus level
154 (Figure 1J). Notably, these altered genera are involved in SCFAs production (Kreznar et al.,
155 2017; Li et al., 2019b; Li et al., 2021; Li et al., 2019c; Bian et al., 2020). These results verify
156 that *MSTN* deficiency can alter the intestinal structure while promoting the growth of
157 microbes related to SCFAs production.

158 **Gut microbiota reshaped by *MSTN* gene deletion promotes fast-twitch glycolytic muscle**
159 **growth**

160 To determine the effect of the *MSTN*-deleted altered intestinal flora on skeletal muscle, we
161 transplanted fecal microbes from $MSTN^{-/-}$ pigs and WT pigs into mice. Mice translated with
162 WT pig feces were named WT-M, and those with $MSTN^{-/-}$ pig feces were named KO-M. After
163 eight weeks of normal chow feeding, KO-M had a higher muscle mass than to WT-M,
164 especially an enlarged gastrocnemius (GA) muscle (Figure 2A). The GA mass, but not that of
165 the soleus (SOL) or extensor digitorum longus (EDL), was significantly enhanced in KO-M
166 than in WT-M (Figure 2B). However, there was no significant difference in food intake,
167 physical activity, energy intake, or absorbed energy between the two mice groups (Figure
168 2-figure supplement 2A-E).

169 Quantitative analysis of fiber size of GA muscle revealed that the CSA of fiber is
170 significantly hypertrophic in KO-M, and that the distribution of fiber sizes in KO-M clearly
171 shifted toward larger fibers (Figure 2C, D). As shown in Figure 2E, the CSA of type IIb
172 myofibers in KO-M was markedly higher than that in WT-M. Correspondingly, the levels of
173 proteins MyHC IIb and MyoD and those of glycolytic enzymes HK2, PFK1 and PKM2 were
174 significantly increased in the GA muscle of KO-M, whereas the levels of MyHC I and IIa were

not significantly different (Figure 2F, G). Interestingly, we observed an increase in Akt and mTOR phosphorylation in the skeletal muscle of KO-M (Figure 2H). The Akt/mTOR signaling pathway affects type IIb myofiber hypertrophy (Izumiya et al., 2008; Dutchak et al., 2018), suggesting an explanation for the increased GA mass in KO-M.

We also performed a series of physiological experiments to evaluate the strength and running performance of fecal microbiota transplantation (FMT) mice. Similar to the expression profile of type IIb myofibers, the grip force of KO-M increased compared with that of WT-M (Figure 2I). However, KO-M had a reduced capacity for running (Figure 2J). Owing to an enlargement in type IIb myofibers, a type of fast-twitch glycolytic muscle, which resulted in a higher explosive force and a lower endurance, KO-M had higher grip strength but shorter running time. Collectively, these observations strongly indicate that KO-M have increased CSA of type IIb myofibers and significantly enhanced fast-twitch glycolytic skeletal muscle mass.

$MSTN^{-/-}$ pigs FMT alter gut microbiota composition in mice

To investigate the correlation between myofiber hypertrophy and intestinal microbiota in mice, we analyzed their intestinal microorganisms. There were no significant differences in the ACE, Chao 1, Shannon, and Simpson indexes for alpha-diversity (Figure 3-figure supplement 3A-D). Principal coordinates analysis (PCoA) showed that the microbiota composition structure of the two groups is clearly differentiated (Figure 3A). In addition, *Romboutsia* was significantly enriched at the order-, family-, genus levels in KO-M intestinal flora (Figure 3B). The heat map showed that abundance of 22 of the 35 increased genera and 13 decreased genera. *Romboutsia*, which was upregulated in $MSTN^{-/-}$ pigs, was also upregulated in KO-M (Figure 3C). KO-M was similar to $MSTN^{-/-}$ pigs, LEfSe analysis showed that *Romboutsia* abundance increased at

the genus level (Figure 3D). Functional prediction analysis showed that intestinal microbial functions are concentrated in pathways related to metabolite synthesis (including K05349 and K01952) in KO-M (Figure 3E). These results showed that the mice translated with *MSTN*$^{-/-}$ pig feces had increased *Romboutsia* abundance in the intestine.

Gut microbes derivative-valeric acid promote myogenic differentiation of myoblasts

As metabolites of the intestinal flora, SCFAs, can affect the growth and function of skeletal muscle (Frampton et al., 2020). The results of our FMT experiments showed that *MSTN* deletion-mediated intestinal microbiota significantly increases skeletal muscle mass and simultaneous enrich *Romboutsia* which can produce SCFAs. Further analysis of fatty acids in the colon contents of mice showed that SCFAs are enriched in KO-M than WT-M; particularly, valeric acid and isobutyric acid were significantly enhanced in KO-M (Figure 4A). However, medium-chain fatty acids (MCFAs) showed no significant differences between the two groups (Figure 4B). Long-chain fatty acids (LCFAs) also showed no difference in WT-M and KO-M overall, although FFA18:2 and FFA16:0 were significantly decreased in KO-M (Figure 4C). The heatmap also confirmed that the differences in SCFAs between WT-M and KO-M (Figure 4D).

To assess the influence of upregulated SCFAs on myoblast differentiation, the C2C12 myoblast cell line was treated for 24 h with 5 mM each of valeric acid and isobutyric acid during differentiation. Immunofluorescence staining of MyHC showed that after supplementation of valeric acid, C2C12 myoblasts produced thicker myotubes and notably higher fusion index than the control cells, implying that valeric acid promotes myotube formation (Figure 5A). Valeric acid treatment also improved the expression of MyoD and

MyoG and promoted the differentiation of C2C12 myoblasts (Figure 5B). Notably, the phosphorylation levels of Akt and mTOR significantly increased after valeric acid treatment (Figure 5C). However, isobutyric acid treatment did not show such effects and only increased the myotube fusion index. Taken together, these results strongly demonstrate that valeric acid can promote myogenic differentiation of myoblasts.

Valeric acid stimulates type IIb myofibers growth

We further elucidated the effect of valeric acid treatment on the phenotype of skeletal muscles *in vivo*. Mice were administered with valeric acid (100 mg/kg) by daily oral gavage. Valeric acid treatment significantly increased the mass of GA muscle, a fast-twitch glycolytic skeletal muscle, compared with the control (Figure 6A, B). Consistently, following valeric acid treatment, the CSA of the GA muscle was significantly larger, and there was a higher proportion of large myofibers compared with the control (Figure 6C). In valeric acid-treated mice, the protein expression of the MyHC IIb was significantly enhanced, that of MyHC I was decreased, and that MyHC IIa showed no change (Figure 6D). In addition, valeric acid treatment significantly upregulated the levels of glycolysis enzymes of HK2, PFK1, and PKM2 (Figure 6E) and the phosphorylation of Akt and mTOR in the GA muscle (Figure 6F).

To explore whether the regulatory pathway, mediated by valeric acid on muscle mass growth would be dependent on fatty acid receptors, we examined the expression of SCFAs receptors in skeletal muscle. Valeric acid increased the mRNA level of *GPR43* in GA muscle, whereas those of *GPR41* and *GPR109a* did not significantly change (Figure 6G). SCFAs could activate the Akt/mTOR pathway through GPR43 (Tang et al., 2022; Brown et al., 2003). These findings suggest that valeric acid, a metabolite of gut microbes, can induce type IIb/glycolytic

myofiber growth and enhance GA mass by activating Akt/mTOR signalling through GPR43. Furthermore, valeric acid-treated mice had a greater grip force (Figure 6H). Interestingly, valeric acid treatment increased the length of the small intestine (Figure 6I), but had no effect on food intake, physical activity, energy intake, or absorbed energy in mice (Figure 6-figure supplement 4A-E).

Valeric acid ameliorates dexamethasone (Dex)-induced skeletal muscle atrophy

Glucocorticoids, such as dexamethasone, are often used to induce muscle atrophy models, and are implicated in protein metabolism in skeletal muscle and are considered as a risk factor for the development of muscle atrophy (Hong et al., 2019; Li et al., 2017). To further explore the role of valeric acid in skeletal muscles, we constructed Dex-induced *in vivo* and *in vitro* muscular atrophy models. Valeric acid administration partially ameliorated skeletal muscle atrophy induced by Dex in mice and reduced the dissolution area with a clear morphology of muscle fiber (Figure 7A). Meanwhile, valeric acid treatment significantly decreased the mRNA and protein levels of muscular dystrophy factors Atrogin-1 and MuRF-1, which were induced by Dex (Figure 7B, C). In C2C12 myoblasts, valeric acid treatment significantly increased myotube diameter and fusion index, and inhibited the expression of atrophy factors, which can improve Dex-induced myotube atrophy (Figure 7D, E). Overall, these finding indicate that valeric acid has a positive effect on Dex-induced muscle atrophy.

Discussion

Host genetic variations can influence the microbiota composition, and the gut microbiota can affect skeletal muscle growth and function. Here, we revealed that the gut microbiota

remodeled by *MSTN* gene deletion plays a key role in regulating skeletal muscle development. *MSTN* gene knockout not only increased skeletal muscle mass, but also altered the intestinal structure and composition of intestinal flora in pigs, as shown the loss of intestinal MSTN expression, altered muscularis thickness, plica length, the increase expression of tight junction genes *ZO-1* and *Occludin*, and enriched microbioal population that produce SCFAs. We transplanted the fecal microbiota of $MSTN^{-/-}$ pigs into mice, and the recipient mice had increased fast-twitch glycolytic muscle GA weight and increased levels of glycolysis proteins HK2, PFK1, and PKM2 and type IIb myofibers hypertrophy, characterized by enhanced grip strength and poor resistance to fatigue, accompanied by increased phosphorylation of the Akt/mTOR signal. Similar to the donor pigs, recipient mice were enriched in microbes that produce SCFAs. Furthermore, metabolomic analysis showed a significant increase in valeric acid levels in the colon contents. We showed that the intestinal flora remodeled by MSTN gene deletion is involved in fast-twitch glycolytic muscle growth via valeric acid, which activaties the Akt/mTOR pathway through the SCFAs receptor GPR43. Lastly, we demonstrated that valeric acid have a beneficial effect on skeletal muscle atrophy induced by Dex (Figure 8).

MSTN regulates myogenic differentiation and skeletal muscle mass mainly by activating classical Smad2/3 transcription factors (Chen et al., 2021). In this study, $MSTN^{-/-}$ pigs generated using TALEN genome editing had significantly inhibited activation of Smad, increased CSA of type IIb myofibers, and overgrowth of skeletal muscle, which was characterized by the ‘double-muscle’ phenotype. These findings are consistent with those of the previous studies performed in *MSTN* mutant mice and cattle (McPherron et al., 1997; Ceccobelli et al., 2022; McPherron and Lee, 1997; Kambadur et al., 1997).

MSTN expression has been detected not only in the skeletal muscles but also in smooth muscles of blood vessels, penis, and other tissues and is co-localized with α-smooth muscle actin, which can affect organ functions (Verzola et al., 2017; Esposito et al., 2020; Kovanecz et al., 2017). Intestine tissues are from smooth muscle, and *MSTN* expression in intestine tissues has been confirmed; however, its role in intestine is not clear (Sundaresan et al., 2008). In this study, MSTN expression was detected in the intestine of WT pigs but not in that of $MSTN^{-/-}$ pigs. Importantly, this is the first study to show that *MSTN* knockout leads to a loss of its expression in the intestine and increases the intestinal muscularis thickness and plica length in pig intestine, indicating *MSTN* knockout-induced changes in intestinal morphology. The muscularis is related to intestinal motility, and its thickness can represent the ability of intestinal peristalsis; the height of the mucosal fold determines the intestinal absorption surface area (Wang et al., 2019; Zhao et al., 2017; Geda et al., 2012). In this study, increases in small intestinal muscularis thickness and plica length imply enhanced intestinal absorptive capacity in $MSTN^{-/-}$ pigs. Actually, *MSTN* gene mutation has also been found to affect the composition of metabolites and microbial strains in the jejunum, which might provide more useable nutrients for the host (Pei et al., 2021). The tight junction between adjacent intestinal epithelial cells is a critical component of the intestinal barrier, which provide a form of cell–cell adhesion in enterocytes and limit the paracellular transport of bacteria and/or bacterial products into the systemic circulation (Ghosh et al., 2020). Previous studies have shown that a disruption in the intestinal barrier leads to increased bacterial products of lipopolysaccharide into systemic circulation, triggering an inflammatory response in specific tissues, such as skeletal muscle or adipose tissue (Ghosh et al., 2020). On the other hand, enhancement of the intestinal barrier

function effectively reduced intestinal inflammation, resulting in the alleviation of skeletal muscle loss in cancer cachexia (Sakakida et al., 2022). In this study, *MSTN*$^{-/-}$ pigs had a significantly increased expression of tight junction genes *ZO-1* and *Occludin* in intestine. It is indicated that *MSTN* gene deletion can improve the intestinal physical barrier of pigs. Importantly, changes in the intestinal environment and barrier function can alter microbial composition of the gut (Seganfredo et al., 2017; Nicoletti et al., 2017; Sekirov et al., 2010). The intestinal microflora composition of *MSTN*$^{-/-}$ pigs was analyzed, and we found that *Romboutsia*, *Treponema*, and *Turicibacter* were significantly enriched. Several studies have suggested that these microbes are involved in SCFAs production (Li et al., 2019b; Li et al., 2021; Li et al., 2019c; Bian et al., 2020). SCFAs are absorbed from the intestinal tract and play a metabolic regulatory role in different organs, which are recognized as a potential regulator of skeletal muscle metabolism and function (Frampton et al., 2020). Additionally, *Romboutsia* (Li et al., 2021; Yanni et al., 2020) and *Turicibacter* (Watanabe et al., 2021) are closely associated with metabolic disorders, such as hypertension, diabetes, dysregulation of skeletal muscle energy metabolism, and obesity. Therefore, we believe that the deletion of the *MSTN* gene in the intestine alters the intestinal structure, thus affecting the composition of intestinal flora.

FMT can transfer both host gut characteristics and metabolic phenotypes from pigs to mice (Yang et al., 2018; Diao et al., 2016; Yan et al., 2016). To verify the effect of the intestinal flora remodeled by *MSTN* gene deletion on skeletal muscle, the intestinal flora of *MSTN*$^{-/-}$ and WT pigs were transplanted into mice. Interestingly, we found that mice transplanted with *MSTN*$^{-/-}$ pigs feces had increased GA muscle mass and muscle fiber area (Figure 2). We

329 further found that the area of type IIb myofibers increased significantly, indicating that the
330 increased GA weight and muscle fiber area can be attributed to the growth of type IIb
331 myofibers. Previous studies have found that Akt1 transgene activation specifically increases
332 GA weight and type IIb myofiber growth through mTOR-dependent pathway (Izumiya et al.,
333 2008). This is consistent with our study, where the significant activation of the Akt1/mTOR
334 pathway was observed with increased GA mass and IIb myofiber CSA in KO-M. In addition,
335 augment of type IIb myofibers lead to an increase in grip strength but a reduction in endurance
336 on a treadmill test (Izumiya et al., 2008). In this study, as expected, KO-M had significantly
337 enhanced grip strength but poor resistance to fatigue. Preservation or restoration of type IIb
338 myofibers may delay age-related changes, mainly by reducing fat mass and liver steatosis and
339 correcting glucose metabolism injury (Akasaki et al., 2014). Importantly, we found that
340 SCFAs producing microbes, *Romboutsia*, enriched in *MSTN*$^{-/-}$ pigs are also significantly
341 enriched in recipient mice (Figure 3B-D). The concentration of SCFAs was significantly
342 increased in the colon contents. Gut microbiota transplantation from pathogen-free mice into
343 germ-free mice was reported to increase skeletal muscle mass and reduce muscle atrophy
344 markers, thus improving oxidative metabolic capacity. Moreover, the microbial
345 metabolites–SCFAs treatment can also attenuate skeletal muscle impairments, especially in the
346 GA muscle (Lahiri et al., 2019). During hibernation, the urease-producing microbes, *Alistipes*,
347 enriched in the gut of ground squirrels can prevent muscle loss (Regan et al., 2022). These
348 results strongly suggest that the intestinal flora remodeled by *MSTN* gene deletion is involved
349 in the growth of fast-twitch glycolytic muscle mass and function, which may be related to the
350 enrichment of SCFAs–producing microbes.

SCFAs are the main metabolites of intestinal microbiota and are involved in multiple physiological processes of the host (Donohoe et al., 2011; Canfora et al., 2015). Compared with untreated mice, SCFAs-treated germ-free mice showed improved muscle strength (Lahiri et al., 2019). In addition, acetic acid, a kind of SCFA, can change fiber types and regulate mitochondrial metabolism of skeletal muscle (Pan et al., 2015). Similarly, we observed that valeric acid treatment increases myotube formation in myoblasts and the skeletal muscle mass of GA in mice, especially with respect to type IIb muscle fiber formation rate. SCFAs play a downstream regulatory role mainly by binding to their receptors (Stoddart et al., 2008; Hul et al., 2019). To explore the possible mechanism of action of valeric acid in skeletal muscles, we analyzed GPRs expression and found a considerable increase in GPR43 levels following valeric acid treatment. The GPR43 receptor can activate the Akt and mTOR signaling pathway (Bian et al., 2020; Dutchak et al., 2018), which may explain the activation of the Akt signaling pathway detected in this study (Figure 6). Aging and long-term and high-dose glucocorticoid therapy could induce skeletal muscle atrophy, mainly manifesting as skeletal muscle mass loss and priority loss of type IIb muscle fibers (Akasaki et al., 2014; Haber et al., 1992; Faulkner et al., 2007; Kirkendall et al., 1998). We found that valeric acid treatment ameliorates Dex-induced myotube atrophy and partially repairs skeletal muscle atrophy (Figure 7).

In conclusion, this is the first study to demonstrate that *MSTN* gene deletion in pig intestine alters intestinal structure and function, leading to changes in the composition of intestinal microbiota. We further demonstrate that *MSTN* gene deletion-mediated remodeling of the intestinal flora increases the growth of fast-twitch glycolytic muscles. Finally, we illustrate that the microbiota metabolite valeric acid can promote myoblast differentiation and fast-twitch

glycolytic myofiber growth by activating the Akt/mTOR pathway through the SCFAs receptor GPR43 and have a beneficial effect for skeletal muscle atrophy induced by Dex. These findings increase our understanding of the host genetic variation in regulating gut microbiota, and provide new insights for the treatment of muscle-related diseases, such as muscular dystrophy and sarcopenia.

Materials and methods

Animals

The animal study was approved by the Ethics Committee of Yanbian University (approval number SYXK2020-0009). We generated *MSTN*$^{-/-}$ pigs with 2 and 4 bp deletions in the two alleles of *MSTN* gene by TALEN genome editing technique and somatic cell nuclear transfer and these pigs were used in this experiment (Kang et al., 2017). Pigs were fed a standard commercial diet and housed in the same environmentally controlled room in a swine breeding farm. Male C57BL/6J mice aged four weeks were purchased from Vital River Laboratory Animal Technology (Beijing, China). Chow diet (Beijing HuaFuKang Bioscience, Beijing, China) and water were provided ad libitum. Mice were administered with valeric acid (100 mg/kg, Shanghai Aladdin, China) by oral gavage or water (vehicle) starting at four weeks of age, and tissues were collected after five weeks of treatment.

To establish the Dex-induced muscle atrophy model, male C57BL/6J mice aged eight weeks were intraperitoneally injected with 20 mg/kg Dex every other day for two weeks, and saline injections were used for the control group. Dex-induced skeletal muscle atrophy was determined by weight loss in mice (Hong et al., 2019; Li et al., 2017). A total of 100 mg/kg of

valeric acid was provided orally to mice every day two weeks before Dex injection until the full experiment cycle. Mice were raised in a pathogen free environment at a controlled ambient 21±1 □, 40–60% relative humidity, and 12/12 h cycle of alternating day and night. In all experiments, the animals were fasted overnight before they were euthanized.

Fecal microbiota transplantation

Fecal samples were collected daily from six-month old *MSTN*$^{-/-}$ and wild-type (WT) donor pigs in the morning. In a sterile environment, they were homogenized and suspended using sterile saline (250 mg/mL), and the mixture was centrifuged at 800 × g for 5 min. Antibiotics mixture (50 μg/mL streptomycin, 100 U/mL penicillin, 170 μg/mL gentamycin, 100 ug/mL metronidazole, 125 ug/mL ciprofloxacin; all from Sigma) was added to sterile drinking water and was given daily for one week before FMT. From five weeks of age, each group of recipient mouse was gavaged with 200 μL of the corresponding bacterial suspension every day for eight weeks until tissue collection.

Analysis of gut microbiota

The fecal samples used for microbiota analysis were collected separately from donor pigs at six-month old and recipient mice after eight weeks of FMT. Methods used to analyze the diversity and taxonomic profiles of gut microbiota in donor pigs and recipient mice have been described previously (Quan et al., 2020). Briefly, the CTAB method was used extract the total genomic DNA from fecal bacteria. DNA sample with a final concentration of 1 ng/μL was used for bacterial 16s rRNA gene amplification seuqnecing (V3-V4 regions). The Illumina NovaSeq platform (Novogene, Beijing, China) was used to determine the sequencing abundance and diversity of the intestinal flora in pigs and mice. The library quality was

417 assessed using a Qubit@ 2.0 Fluorometer (Thermo Scientific) and Agilent Bioanalyzer 2100
418 system.

419 Paired-end reads were allocated according to the unique barcodes of the sample and
420 truncated by cutting off the barcode and primer sequences. FLASH (v1.2.7) was used to
421 merge the overlapped reads between paired-end reads. According to the QIIME (V1.9.1)
422 quality control process, high-quality clean tags were obtained from qualitative filtration of the
423 original reads under specific filtration conditions. The effective tags were finally collected by
424 comparing the sample tags with the reference database (Silva database) after the detection and
425 removal of chimera sequences using the UCHIME algorithm. The QIIME software was used
426 to calculate all indices in the samples, and R (v2.15.3) was used for bioinformatic analyses of
427 the sequences. The same operational taxonomic units had at least 97% similarity in sequences.
428 Alpha diversity, beta diversity, and principal component analysis (PCA) were described
429 according to the unweighted unifrac distances.

430 **Cell culture**

431 C2C12 myoblasts (1×10^5 cells/well) were cultured in six-well culture plates in Dulbecco's
432 modified Eagle's medium (DMEM; Invitrogen-Gibco), containing 10% fetal bovine serum
433 (Sigma), 100 U/mL penicillin and 100 U/mL streptomycin (Invitrogen-Gibco) for
434 proliferation. For differentiation, C2C12 myoblasts at 80% confluence were induced to
435 differentiate in DMEM with 2% horse serum (Invitrogen); valeric acid and isobutyric acid
436 were added to the differentiation medium for 24 h. Cells were supplemented with a fresh
437 differentiation medium every two days. Myotubes were obtained on day 5 of the
438 differentiation phase.

To establish the Dex-induced myotube atrophy model, myoblasts were treated with 100 μm/L of Dex at the beginning of differentiation for 24 h, and 5 mM/L valeric acid was added to the treatment group. Myoblasts were cultured in a fresh differentiation medium for five days. Myotubes were stained with anti-MyHC antibody (MyHC, A4.1025, Sigma), and Alexa Fluor 488-labelled goat anti-mouse IgG was used as secondary antibody (Jackson ImmunoResearch Laboratories). The nuclei were counterstained with 10 μg/μL DAPI (D-9106, Beijing Bioss Biotechnology). The diameter and the number of nuclei of the differentiated myotubes were measured using Image J (1.51q, National Institutes of Health, USA). For each group, five pictures were randomly taken from each well of the six-well plates. The diameters of the three different parts of each myotube were measured, and the average value was calculated. To determine the C2C12 fusion index, the number of nuclei in the myotubes were calculated and divided by the total number of nuclei and multiplied by 100.

Histological analysis

Skeletal muscle and intestine morphology were detected by hematoxylin eosin (HE) staining. The longissimus dorsi and intestine tissues from *MSTN*$^{-/-}$ and WT pigs were from 5 μm thick paraffin-embedded sections. Images were obtained using a light microscope (BX53, Olympus, Japan).

Liquid nitrogen-cooled isopentane was used to rapid freeze the skeletal muscle tissues, which were embedded in the OCT compound (Sakura Finetech USA Inc.). Cryostat sections (10 μm) were prepared from the mid-belly of the muscle tissue. Fiber-type of skeletal muscle was stained using MyHC type I (BA-D5, DSHB, Douglas Houston), MyHC type IIa (SC-71,

DSHB, Douglas Houston), MyHC type IIb (BF-F3, DSHB, Douglas Houston), and laminin (ab11575, Abcam) monoclonal antibodies. Alexa Fluor 647 conjugate goat anti-mouse IgG2b, Alexa Fluor 488 conjugate goat anti-mouse IgG1, Alexa Fluor 555 conjugate goat anti-mouse IgM, or Alexa Fluor 594 conjugate goat anti-rabbit IgG were used as secondary antibodies. The nuclei were counterstained with 10 μg/μL of DAPI. Fluorescence was detected using a confocal laser scanning microscope (FV3000, Olympus, Japan). Image J software was used to measure the thickness and the cross-sectional area (CSA) of the myofibers. The damage area of skeletal muscle fiber was evaluated by calculating the ratio of muscle fiber ablation area to the total muscle fiber CSA.

Quantitative real-time PCR

Total RNA was extracted from liquid nitrogen quick-frozen tissue using a Total RNA Extraction Kit (LS1040; Promega) as per the manufacturer's protocol. After evaluating the concentration and purity of RNA, an equal amount of RNA was used for reverse transcription. Information on the primers used is available in supplementary materials. Real-time PCR was performed on Mx3005P system (Agilent, Santa Clara, CA, USA), and the relative gene expression levels were calculated using the $2^{-\Delta\Delta CT}$ method and normalized to that of the control group.

Western blotting

The cells and tissues were homogenized in RIPA buffer (Beyotime). Equal amounts of protein were calculated and loaded according to the concentration of protein that was detected by a BCA kit (Beyotime, Shanghai, China). Subsequently, immunoblot analysis was performed following standard procedures. Protein samples were electrophoresed, transferred, blocked

and incubated with the following primary antibodies: phospho-Akt (Ser473), phospho-mTOR (Ser2448), phospho-Smad2 (Ser465/467)/Smad3 (Ser423/425), Akt, mTOR, Smad2/3, and HK2 from Cell Signaling Technology; PFK1 and PKM2 from Shanghai Absin, Inc.; MyHC type I, MyHC type Iia, and MyHC type IIb from DSHB; MSTN, MyoD, MyoG, α-SMA, calponin-1, MuRF-1, atrogin-1, actin, and tubulin from Beijing Bioss Biotechnology, Inc.. The ChemiDoc™ MP Imaging System and Image Lab software (Bio-Rad, Shanghai, China) were used to analyze the blot bands.

SCFAs analysis

Colon contents were collected at the time of mouse tissue sample collection after eight weeks of FMT. SCFAs were extracted from mouse feces using 1:1 acetonitrile:water solution and derivatized using 3-nitrophenylhdyrazones. SCFAs were analyzed using a Jasper HPLC coupled to a Sciex 4500 MD system (LipidALL Technologies Co., Ltd, Changzhou, China). In brief, a Phenomenex Kinetex C_{18} column (100 × 2.1 mm, 2.6 µm) was used to separate individual SCFA. The mobile phase A consisted of 0.1% formic acid aqueous solution, and the mobile phase B consisted of 0.1% formic acid acetonitrile. Octanoic acid-1-$^{13}C_1$ (Sigma-Aldrich) and butyric-2,2-d_2 (CDN Isotopes) were used as internal standards for quantitation (Li et al., 2019a).

Statistical analysis

Statistical analysis was performed using SPSS (17.0, IBM, Armonk, NY, USA) and GraphPad Prism (San Diego, CA, USA). Data are presented as the mean ± SEM, and were compared using a repeated measure two-way analysis of variance (ANOVA), one-way ANOVA, or Student's *t-test*. Statistical significance was set at $*P<0.05$, $**P<0.01$, $***P<0.001$.

Acknowledgments

The author would like to appreciate Yanbian University for its support to Tumen River Scholars.

Additional information

Competing interests

The authors declare that they have no competing interests.

Funding

This work was supported by the 13th Five-Year Plan Science and Technology Research Project of Education Department of Jilin Province of China (JJKH20200520KJ, JJKH20210586KJ); Innovative and Entrepreneurial Talent in Jilin Province of China (2020022); the Higher Education Discipline Innovation Project (111 Project, D18012).

Author contributions

L-HQ, J-DK, Z-BL and X-JY conceived the project, contributed to experimental design; L-HQ, J-DK, Z-BL and SH performed experiments, interpreted the results, prepared the figures and wrote the manuscript; SH, HL and H-LL contributed to writing and editing; JW, CH, DW, YL and DL performed animal studies; Z-BL, KG and BQ performed animal tissue analysis; SC and MX performed cellular experiments; all authors discussed the results and approved the manuscript.

Ethics approval and consent to participate

The animal study was approved by the Ethics Committee of Yanbian University (approval number SYXK2020-0009).

Additional files

Supporting information

Supplementary Figures and Table.

Supplementary methods.

Availability of data and materials

The raw reads of 16s rRNA gene sequences have been submitted to the NCBI BioSample database (Porcine data: PRJNA743164; Mice data: PRJNA743401).

All sample metadata and intermediate analysis files are available at https://www.scidb.cn/s/YRZ32q.

549 **References**

550 Agus A, Clément K, Sokol H. 2021. Gut microbiota-derived metabolites as central regulators
551 in metabolic disorders. *Gut* **70**, 1174-1182. DOI: https://doi:10.1136/gutjnl-2020-323071,
552 PMID: 33272977

553 Agus A, Planchais J, Sokol H. 2018. Gut Microbiota Regulation of Tryptophan Metabolism in
554 Health and Disease. *Cell Host Microbe* **23**, 716-724. DOI:
555 https://doi:10.1016/j.chom.2018.05.003, PMID: 29902437

556 Akasaki Y, Ouchi N, Izumiya Y, Bernardo BL, Lebrasseur NK, Walsh K. 2014. Glycolytic
557 fast-twitch muscle fiber restoration counters adverse age-related changes in body
558 composition and metabolism. *Aging cell* **13**, 80-91. DOI: https://doi:10.1111/acel.12153,
559 PMID: 24033924

560 Bassel-Duby R, Olson EN. 2006. Signaling pathways in skeletal muscle remodeling. *Annu.*
561 *Rev. Biochem* **75**, 19-37. DOI: https://doi:10.1146/annurev.biochem.75.103004.142622,
562 PMID: 16756483

563 Besten Gd, Eunen Kv, Groen AK, Venema K, Reijngoud DJ, Bakker BM. 2013. The role of
564 short-chain fatty acids in the interplay between diet, gut microbiota, and host energy
565 metabolism. *J. Lipid. Res* **54**, 2325-2340. DOI: https://doi:10.1194/jlr.R036012, PMID:
566 23821742

567 Bian X, Yang L, Wu W, Lv L, Jiang X, Wang Q, Wu J, Li Y, Ye J, Fang D, Shi D, Wang K,
568 Wang Q, Lu Y, Xie J, Xia J, Li L. 2020. Pediococcus pentosaceus LI05 alleviates
569 DSS-induced colitis by modulating immunological profiles, the gut microbiota and
570 short-chain fatty acid levels in a mouse model. *Microb. Biotechnol* **13**, 1228-1244. DOI:

https://doi:10.1111/1751-7915.13583, PMID: 32363766

Brown AJ, Goldsworthy SM, Barnes AA, Eilert MM, Tcheang L, Daniels D, Muir AI, Wigglesworth MJ, Kinghorn I, Fraser NJ, Pike NB, Strum JC, Steplewski KM, Murdock PR, Holder JC, Marshall FH, Szekeres PG, Wilson S, Ignar DM, Foord SM, Wise A, Dowell SJ. 2003. The Orphan G protein-coupled receptors GPR41 and GPR43 are activated by propionate and other short chain carboxylic acids. *J. Biol. Chem* **278**, 11312-11319. DOI: https://doi:10.1074/jbc.M211609200, PMID: 12496283

Canfora EE, Jocken JW, Blaak EE. 2015. Short-chain fatty acids in control of body weight and insulin sensitivity. *Nat. Rev. Endocrinol* **11**, 577-591. DOI: https://doi:10.1038/nrendo.2015.128, PMID: 26260141

Ceccobelli S, Perini F, Trombetta MF, Tavoletti S, Lasagna E, Pasquini M. 2022. Effect of Myostatin Gene Mutation on Slaughtering Performance and Meat Quality in Marchigiana Bulls. *Animals* **12**, 518-529. DOI: https://doi: 10.3390/ani12040518, PMID: 35203227

Chen F, Li Q, Chen Y, Wei Y, Liang J, Song Y, Shi l, Wang J, Mao L, Zhang B, Zhang Z. 2022. Association of the gut microbiota and fecal short-chain fatty acids with skeletal muscle mass and strength in children. *FASEB J* **36**, e22109. DOI: https://doi:10.1096/fj.202002697RRR, PMID: 34941012

Chen MM, Zhao YP, Zhao Y, Deng SL, Yu K. 2021. Regulation of Myostatin on the Growth and Development of Skeletal Muscle. *Front Cell Dev Biol* **9**, 785712. DOI: https://doi: 10.3389/fcell.2021.785712, PMID: 35004684

Cho MR, Lee S, Song SK. 2022. A Review of Sarcopenia Pathophysiology, Diagnosis, Treatment and Future Direction. *J. Korean. Med. Sci.* **37**, e146. DOI:

https://doi:10.3346/jkms.2022.37.e146, PMID: 35535373

Diao H, Yan HL, Xiao Y, Yu B, Yu J, He J, Zheng P, Zeng BH, Wei H, Mao XB, Chen DW. 2016. Intestinal microbiota could transfer host Gut characteristics from pigs to mice. *BMC Microbiol* **16**, 238-253. DOI: https://doi:10.1186/s12866-016-0851-z, PMID: 27729007

Donohoe DR, Garge N, Zhang X, Sun W, O'Connell TM, Bunger MK, Bultman SJ. 2011. The microbiome and butyrate regulate energy metabolism and autophagy in the mammalian colon. *Cell Metab* **13**, 517-526. DOI: https://doi:10.1016/j.cmet.2011.02.018, PMID: 21531334

Dutchak PA, Estill-Terpack SJ, Plec AA, Zhao X, Yang C, Chen J, Ko B, Deberardinis RJ, Yu Y, Tu BP. 2018. Loss of a Negative Regulator of mTORC1 Induces Aerobic Glycolysis and Altered Fiber Composition in Skeletal Muscle. *Cell Rep* **23**, 1907-1914. DOI: https://doi:10.1016/j.celrep.2018.04.058, PMID: 29768191

Esposito P, Verzola D, Porta E, Milanesi S, Grignano MA, Avella A, Gregorini M, Abelli M, Ticozzelli E, Rampino T, Garibotto G. 2020. Myostatin in the Arterial Wall of Patients with End-Stage Renal Disease. *J. Atheroscler. Thromb* **27**, 1039-1052. DOI: https://doi:10.5551/jat.51144, PMID: 32173683

Faulkner JA, Larkin LM, Claflin DR, Brooks SV. 2007. Age-related changes in the structure and function of skeletal muscles. *Clin. Exp. Pharmacol. Physiol* **34**, 1091-1096. DOI: https://doi:10.1111/j.1440-1681.2007.04752.x, PMID: 17880359

Frampton J, Murphy KG, Frost G, Chambers ES. 2020. Short-chain fatty acids as potential regulators of skeletal muscle metabolism and function. *Nat. Metab* **2**, 840-848. DOI: https://doi:10.1038/s42255-020-0188-7, PMID: 32694821

615 Geda F, Rekecki A, Decostere A, Bossier P, Wuyts B, Kalmar ID, Janssens GPJ. 2012.
616 Changes in intestinal morphology and amino acid catabolism in common carp at mildly
617 elevated temperature as affected by dietary mannanoligosaccharide. *Anim. Feed Sci. Technol*
618 **178**, 95-102. DOI: https://doi.10.1016/j.anifeedsci.2012.09.008
619 Ghosh SS, Wang J, Yannie PJ, Ghosh S. 2020. Intestinal Barrier Dysfunction, LPS
620 Translocation, and Disease Development. *J. Endocr. Soc* **4**, bvz039. DOI:
621 https://doi:10.1210/jendso/bvz039, PMID: 32099951
622 Haber RS, Weinstein SP. 1992. Role of glucose transporters in glucocorticoid-induced insulin
623 resistance. GLUT4 isoform in rat skeletal muscle is not decreased by dexamethasone.
624 *Diabetes* **41**, 728-735. DOI: https://doi:10.2337/diab.41.6.728, PMID: 1587399
625 He QW, Zhang Y, Ma D, Zhang WQ, Zhang HP. 2022. Lactobacillus casei Zhang exerts
626 anti-obesity effect to obese glut1 and gut-specific-glut1 knockout mice via gut microbiota
627 modulation mediated different metagenomic pathways. *European journal of nutrition* **61**,
628 2003-2014. DOI: https://doi:10.1007/s00394-021-02764-0, PMID: 34984487
629 Hong Y, Lee JH, Jeong KW, Choi CS, Jun HS. 2019. Amelioration of muscle wasting by
630 glucagon-like peptide-1 receptor agonist in muscle atrophy. *J. Cachexia Sarcopenia Muscle*
631 **10**, 903-918. DOI: https://doi:10.1002/jcsm.12434, PMID: 31020810
632 Hul MV, Cani PD. 2019. Targeting Carbohydrates and Polyphenols for a Healthy Microbiome
633 and Healthy Weight. *Curr. Nutr. Rep* **8**, 307-316. DOI:
634 https://doi:10.1007/s13668-019-00281-5, PMID: 31161579
635 Izumiya Y, Hopkins T, Morris C, Sato K, Zeng L, Viereck J, Hamilton JA, Ouchi N,
636 LeBrasseur NK, Walsh K. 2008. Fast/Glycolytic muscle fiber growth reduces fat mass and

637 improves metabolic parameters in obese mice. *Cell Metab* **7**, 159-172. DOI:
638 https://doi:10.1016/j.cmet.2007.11.003, PMID: 18249175

639 Kambadur R, Sharma M, Smith TP, Bass JJ. 1997. Mutations in myostatin (GDF8) in
640 double-muscled Belgian Blue and Piedmontese cattle. *Genome Res* **7**, 910-916. DOI:
641 https://doi:10.1101/gr.7.9.910, PMID: 9314496

642 Kang JD, Kim S, Zhu HY, Jin L, Guo Q, Li XC, Zhang YC, Xing XX, Xuan MF, Zhang GL,
643 Luo QR, Kim YS, Cui CD, Li WX, Cui ZY, Kim JS, Yin XJ. 2017. Generation of cloned
644 adult muscular pigs with myostatin gene mutation by genetic engineering. *RSC Advances* **7**,
645 12541-12549. DOI: https://doi:10.1039/C6RA28579A

646 Kelleher SL, Alam S, Rivera OC, Barber-Zucker S, Zarivach R, Wagatsuma T, Kambe T,
647 Soybel DI, Wright J, Lamendella R. 2022. Loss-of-function SLC30A2 mutants are
648 associated with gut dysbiosis and alterations in intestinal gene expression in preterm infants.
649 *Gut. Microbes* **14**, 2014739. DOI: https://doi:10.1080/19490976.2021.2014739, PMID:
650 34965180

651 Kim JW, Kim R, Choi H, Lee SJ, Bae GU. 2021. Understanding of sarcopenia: from
652 definition to therapeutic strategies. *Arch. Pharma. Res* **44**, 876-889. DOI:
653 https://doi:10.1007/s12272-021-01349-z, PMID: 34537916

654 Kirkendall DT, Garrett WE Jr. 1998. The effects of aging and training on skeletal muscle. *Am*
655 *J Sports Med* **26**, 598-602. DOI: https://doi:10.1177/03635465980260042401, PMID:
656 9689386

657 Kovanecz I, Masouminia M, Gelfand R, Vernet D, Rajfer J, Gonzalez-Cadavid NF. 2017.
658 Myostatin, a profibrotic factor and the main inhibitor of striated muscle mass, is present in

659 the penile and vascular smooth muscle. *Int. J. Impot. Res* **29**, 194-201. DOI:
660 https://doi:10.1038/ijir.2017.22, PMID: 28539643

661 Kreznar JH, Keller MP, Traeger LL, Rabaglia ME, Schueler KL, Stapleton DS, Zhao W,
662 Vivas EI, Yandell BS, Broman AT, Hagenbuch B, Attie AD, Rey FE. 2017. Host Genotype
663 and Gut Microbiome Modulate Insulin Secretion and Diet-Induced Metabolic Phenotypes.
664 *Cell Rep* **18**, 1739-1750. DOI: https://doi:10.1016/j.celrep.2017.01.062, PMID: 28199845

665 Lahiri S, Kim H, Garcia-Perez I, Reza MM, Martin KA, Kundu P, Cox LM, Selkrig J, Posma
666 JM, Zhang H, Padmanabhan P, Moret C, Gulyás B, Blaser MJ, Auwerx J, Holmes E,
667 Nicholson J, Wahli W, Pettersson S. 2019. The gut microbiota influences skeletal muscle
668 mass and function in mice. *Sci. Transl. Med* **11**, eaan5662. DOI:
669 https://doi:10.1126/scitranslmed.aan5662, PMID: 31341063

670 Li B, Li L, Li M, Lam SM, Wang G, Wu Y, Zhang H, Niu C, Zhang X, Liu X, Hambly C, Jin
671 W, Shui G, Speakman JR. 2019a. Microbiota Depletion Impairs Thermogenesis of Brown
672 Adipose Tissue and Browning of White Adipose Tissue. *Cell Rep* **26,** 2720-2737. DOI:
673 https://doi:10.1016/j.celrep.2019.02.015, PMID: 30840893

674 Li H, Li H, Xie P, Li Z, Yin Y, Blachier F, Kong X. 2019b. Dietary supplementation with
675 fermented Mao-tai lees beneficially affects gut microbiota structure and function in pigs.
676 *AMB Express* **9**, 26-39. DOI: https://doi:10.1186/s13568-019-0747-z, PMID: 30778768

677 Li J, Chan MC, Yu Y, Bei Y, Chen P, Zhou Q, Cheng L, Chen L, Ziegler O, Rowe GC, Das S,
678 Xiao J. 2017. miR-29b contributes to multiple types of muscle atrophy. *Nat. Commun* **8**,
679 15201. DOI: https://doi:10.1038/ncomms15201, PMID: 28541289

680 Li JW, Fang B, Pang GF, Zhang M, Ren FZ. 2019c. Age- and diet-specific effects of chronic

681 exposure to chlorpyrifos on hormones, inflammation and gut microbiota in rats. *Pestic.*
682 *Biochem. Physiol* **159**, 68-79. DOI: https://doi:10.1016/j.pestbp.2019.05.018, PMID:
683 31400786

684 Li Y, Zafar S, Salih Ibrahim RM, Chi HL, Xiao T, Xia WJ, Li HB, Kang YM. 2021. Exercise
685 and food supplement of vitamin C ameliorate hypertension through improvement of gut
686 microflora in the spontaneously hypertensive rats. *Life Sci* **269**, 119097. DOI:
687 https://doi:10.1016/j.lfs.2021.119097, PMID: 33482189

688 Lv WQ, Lin X, Shen H, Liu HM, Qiu X, Li BY, Shen WD, Ge CL, Lv FY, Shen J, Xiao HM,
689 Deng HW. 2021. Human gut microbiome impacts skeletal muscle mass via gut microbial
690 synthesis of the short-chain fatty acid butyrate among healthy menopausal women. *J.*
691 *Cachexia Sarcopenia Muscle* **12**, 1860-1870. DOI: https://doi:10.1002/jcsm.12788, PMID:
692 34472211

693 McPherron AC, Lawler AM, Lee SJ. 1997. Regulation of skeletal muscle mass in mice by a
694 new TGF-beta superfamily member. *Nature* **387**, 83-90. DOI: https://doi: 10.1038/387083a0,
695 PMID: 9139826

696 McPherron AC, Lee SJ. 1997. Double muscling in cattle due to mutations in the myostatin
697 gene. *Proc. Natl. Acad. Sci. USA* **94**, 12457-12461. DOI:
698 https://doi:10.1073/pnas.94.23.12457, PMID: 9356471

699 Meng ZX, Li S, Wang L, Ko HJ, Lee Y, Jung DY, Okutsu M, Yan Z, Kim JK, Lin JD. 2013.
700 Baf60c drives glycolytic metabolism in the muscle and improves systemic glucose
701 homeostasis through Deptor-mediated Akt activation. *Nat. Med* **19**, 640-645. DOI:
702 https://doi:10.1038/nm.3144, PMID: 23563706

703 Mosher DS, Quignon P, Bustamante CD, Sutter NB, Mellersh CS, Parker HG, Ostrander EA.
704 2007. A mutation in the myostatin gene increases muscle mass and enhances racing
705 performance in heterozygote dogs. *PLoS Genet* **3**, e79. DOI:
706 https://doi:10.1371/journal.pgen.0030079, PMID: 17530926
707 Newman AB, Kupelian V, Visser M, Simonsick EM, Goodpaster BH, Kritchevsky SB,
708 Tylavsky FA, Rubin SM, Harris TB. 2006. Strength, but not muscle mass, is associated with
709 mortality in the health, aging and body composition study cohort. *J. Gerontol A. Biol. Sci.*
710 *Med. Sci* **61**, 72-77. DOI: https://doi: 10.1093/gerona/61.1.72, PMID: 16456196
711 Nicoletti CF, Cortes-Oliveira C, Pinhel MAS, Nonino CB. 2017. Bariatric Surgery and
712 Precision Nutrition. *Nutrients* **9**, 974-987. DOI: https://doi:10.3390/nu9090974, PMID:
713 28878180
714 Pan JH, Kim JH, Kim HM, Lee ES, Shin DH, Kim S, Shin M, Kim SH, Lee JH, Kim YJ.
715 2015. Acetic acid enhances endurance capacity of exercise-trained mice by increasing
716 skeletal muscle oxidative properties. *Biosci Biotechnol Biochem* **79**, 1535-1541. DOI:
717 https://doi:10.1080/09168451.2015.1034652, PMID: 26000971
718 Pei Y, Chen C, Mu Y, Yang Y, Feng Z, Li B, Li H, Li K. 2021. Integrated Microbiome and
719 Metabolome Analysis Reveals a Positive Change in the Intestinal Environment of *Myostatin*
720 Edited Large White Pigs. *Front. Microbiol* **12,** 628685. DOI:
721 https://doi:10.3389/fmicb.2021.628685, PMID: 33679652
722 Quan LH, Zhang C, Dong M, Jiang J, Xu H, Yan C, Liu X, Zhou H, Zhang H, Chen L, Zhong
723 FL, Luo ZB, Lam SM, Shui G, Li D, Jin W. 2020. Myristoleic acid produced by enterococci
724 reduces obesity through brown adipose tissue activation. *Gut* **69**, 1239-1247. DOI:

https://doi:10.1136/gutjnl-2019-319114, PMID: 31744910

Regan MD, Chiang E, Liu YX, Tonelli M, Verdoorn KM, Gugel SR, Suen G, Carey HV, Assadi-Porter FM. 2022. Nitrogen recycling via gut symbionts increases in ground squirrels over the hibernation season. *Science* **28**, 460-463. DOI: https://doi:10.1126/science.abh2950, PMID: 35084962

Sakakida T, Ishikawa T, Doi T, Morita R, Endo Y, Matsumura S, Ota T, Yoshida J, Hirai Y, Mizushima K, Higashimura Y, Inoue K, Okayama T, Uchiyama K, Takagi T, Abe A, Inoue R, Itoh Y, Naito Y. 2022. Water-soluble dietary fiber alleviates cancer-induced muscle wasting through changes in gut microenvironment in mice. *Cancer Sci* **113**, 1789-1800. DOI: https://doi:10.1111/cas.15306, PMID: 35201655

Scheiman J, Luber JM, Chavkin TA, Donald TM, Tung A, Pham LD, Wibowo MC, Wurth RC, Punthambaker S, Tierney BT, Yang Z, Hattab MW, Avila-Pacheco J, Clish CB, Lessard S, Church GM, Kostic AD. 2019. Meta-omics analysis of elite athletes identifies a performance-enhancing microbe that functions via lactate metabolism. *Nat. Med* **25**, 1104-1109. DOI: https://doi:10.1038/s41591-019-0485-4, PMID: 31235964

Schiaffino S, Reggiani C. 2011. Fiber types in mammalian skeletal muscles. *Physiol. Rev* **91**, 1447-1531. DOI: https://doi:10.1152/physrev.00031.2010, PMID: 22013216

Schuelke M, Wagner KR, Stolz LE, Hübner C, Riebel T, Kömen W, Braun T, Tobin JF, Lee SJ. 2004. Myostatin mutation associated with gross muscle hypertrophy in a child. *N. Engl. J. Med* **350**, 2682-2688. DOI: https://doi:10.1056/NEJMoa040933, PMID: 15215484

Seganfredo FB, Blume CA, Moehlecke M, Giongo A, Casagrande DS, Spolidoro JVN, Padoin AV, Schaan BD, Mottin CC. 2017. Weight-loss interventions and gut microbiota

747 changes in overweight and obese patients: a systematic review. *Obes. Rev* **18**, 832-851. DOI:
748 https://doi:10.1111/obr.12541, PMID: 28524627
749 Sekirov I, Russell SL, Antunes LC, Finlay BB. 2010. Gut microbiota in health and disease.
750 *Physiol. Rev* **90**, 859-904. DOI: https://doi:10.1152/physrev.00045.2009, PMID: 20664075
751 Sovran B, Hugenholtz F, Elderman M, Van Beek AA, Graversen K, Huijskes M, Boekschoten
752 MV, Savelkoul HFJ, De Vos P, Dekker J, Wells JM. 2019. Age-associated Impairment of the
753 Mucus Barrier Function is Associated with Profound Changes in Microbiota and Immunity.
754 *Sci. Rep* **9**, 1437-1450. DOI: https://doi:10.1038/s41598-018-35228-3, PMID: 30723224
755 Srikanthan P, Karlamangla AS. 2014. Muscle mass index as a predictor of longevity in older
756 adults. *Am J Med* **127**, 547-553. DOI: https://doi: 10.1016/j.amjmed.2014.02.007, PMID:
757 24561114
758 Stoddart LA, Smith NJ, Milligan G. 2008. International Union of Pharmacology. LXXI. Free
759 fatty acid receptors FFA1, -2, and -3: pharmacology and pathophysiological functions.
760 *Pharmacol. Rev* **60**, 405-417. DOI: https://doi:10.1124/pr.108.00802, PMID: 19047536
761 Sundaresan NR, Saxena VK, Singh R, Jain P, Singh KP, Anish D, Singh N, Saxena M, Ahmed
762 KA. 2008. Expression profile of myostatin mRNA during the embryonic organogenesis of
763 domestic chicken (Gallus gallus domesticus). *Res. Vet. Sci* **85**, 86-91. DOI:
764 https://doi:10.1016/j.rvsc.2007.09.014, PMID: 18037460
765 Swindle MM, Makin A, Herron AJ, Clubb Jr. FJ, Frazier KS. 2012. Swine as models in
766 biomedical research and toxicology testing. *Vet. Pathol* **49**, 344-356. DOI:
767 https://doi:10.1177/0300985811402846, PMID: 21441112
768 Tang G, Du Y, Guan H, Jia J, Zhu N, Shi Y, Rong S, Yuan W. 2022. Butyrate ameliorates

769 skeletal muscle atrophy in diabetic nephropathy by enhancing gut barrier function and
770 FFA2-mediated PI3K/Akt/mTOR signals. *Br. J. Pharmacol* **179**, 159-178. DOI:
771 https://doi:10.1111/bph.15693, PMID: 34638162

772 Verbrugge SAJ, Gehlert S, Stadhouders LEM, Jacko D, Aussieker T, Wit GMJd, Vogel ISP,
773 Offringa C, Schönfelder M, Jaspers RT, Wackerhage H. 2020. PKM2 Determines Myofiber
774 Hypertrophy In Vitro and Increases in Response to Resistance Exercise in Human Skeletal
775 Muscle. *Int. J. Mol. Sci* **21**, 7062-7077. DOI: https://doi:10.3390/ijms21197062, PMID:
776 32992783

777 Verzola D, Milanesi S, Bertolotto M, Garibaldi S, Villaggio B, Brunelli C, Balbi M, Ameri P,
778 Montecucco F, Palombo D, Ghigliotti G, Garibotto G, Lindeman JH, Barisione C. 2017.
779 Myostatin mediates abdominal aortic atherosclerosis progression by inducing vascular
780 smooth muscle cell dysfunction and monocyte recruitment. *Sci. Rep* **7**, 46362. DOI:
781 https://doi:10.1038/srep46362, PMID: 28406165

782 Wang Y, Yan X, Zhang W, Liu Y, Han D, Teng K, Ma Y. 2019. Lactobacillus casei Zhang
783 Prevents Jejunal Epithelial Damage to Early-Weaned Piglets Induced by Escherichia coli
784 K88 via Regulation of Intestinal Mucosal Integrity, Tight Junction Proteins and Immune
785 Factor Expression. *J. Microbiol. Biotechnol* **29**, 863-876. DOI:
786 https://doi:10.4014/jmb.1903.03054, PMID: 31091863

787 Watanabe K, Katagiri S, Takahashi H, Sasaki N, Maekawa S, Komazaki R, Hatasa M,
788 Kitajima Y, Maruyama Y, Shiba T, Komatsu K, Ohsugi Y, Tanaka K, Matsuzawa A, Hirota T,
789 Tohara H, Eguchi Y, Anzai K, Hattori A, Iwata T. 2021. Porphyromonas gingivalis impairs
790 glucose uptake in skeletal muscle associated with altering gut microbiota. *FASEB J* **35**,

e21171. DOI: https://doi:10.1096/fj.202001158R, PMID: 33197074

Yan H, Diao H, Xiao Y, Li W, Yu B, He J, Yu J, Zheng P, Mao X, Luo Y, Zeng B, Wei H, Chen D. 2016. Gut microbiota can transfer fiber characteristics and lipid metabolic profiles of skeletal muscle from pigs to germ-free mice. *Sci Rep* **6**, 31786-31797. DOI: https://doi:10.1038/srep31786, PMID: 27545196

Yang H, Xiang Y, Robinson K, Wang J, Zhang G, Zhao J, Xiao Y. 2018. Gut Microbiota Is a Major Contributor to Adiposity in Pigs. *Front. Microbiol* **9**, 3045-3057. DOI: https://doi:10.3389/fmicb.2018.03045, PMID: 30619136

Yanni AE, Mitropoulou G, Prapa I, Agrogiannis G, Kostomitsopoulos N, Bezirtzoglou E, Kourkoutas Y, Karathanos VT. 2020. Functional modulation of gut microbiota in diabetic rats following dietary intervention with pistachio nuts (Pistacia vera L.). *Metabol. Open* **7**, 100040-100052. DOI: https://doi:10.1016/j.metop.2020.100040, PMID: 32812934

Zhao Z, Song F, Xu Q. 2017. Effects of glutamine and its precursors on the growth performance and relevant protein synthesis pathway of mirror carp Cyprinus carpio. Fisheries Science 83, 1019-1026. DOI: https://doi:10.1007/s12562-017-1124-y

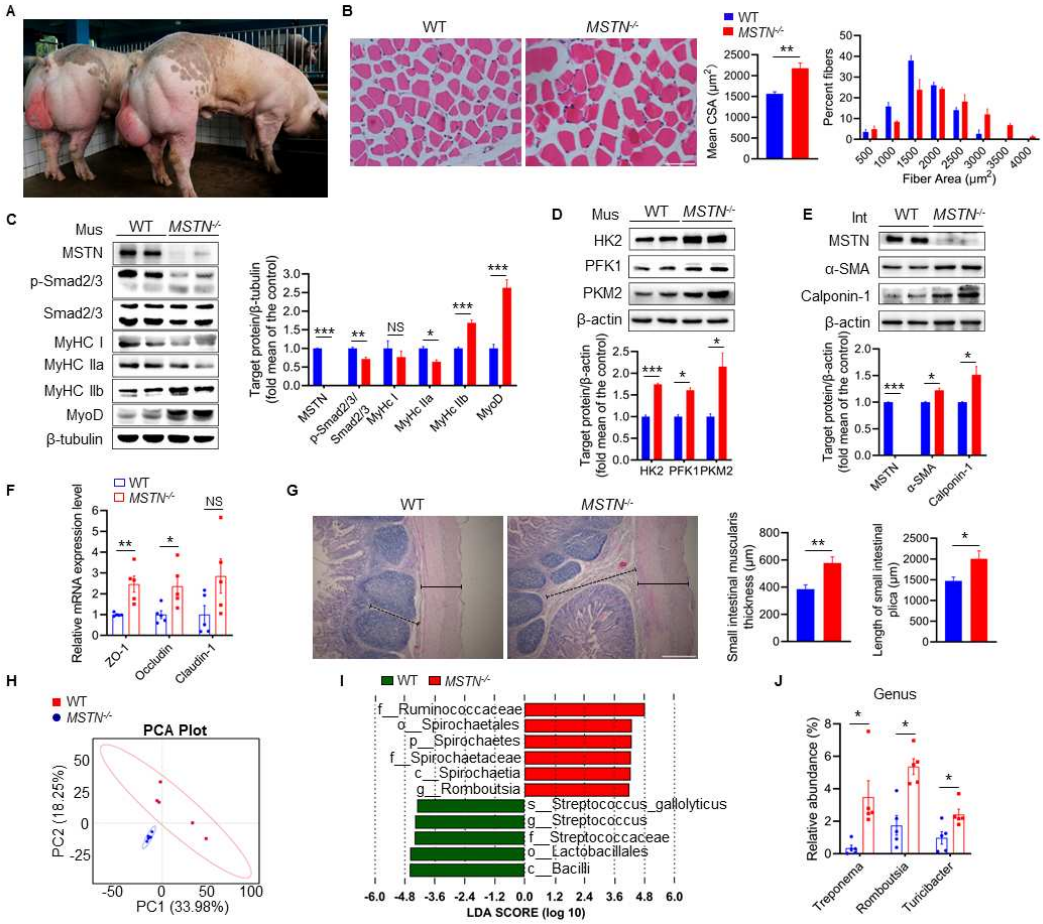

Figure 1. *MSTN* deletion stimulates muscle hypertrophy and alters intestinal structure and composition of gut microbiota in pigs (n=5). (**A** and **B**) Representative images of *MSTN*$^{-/-}$ pigs and hematoxylin eosin staining longissimus dorsi. Magnification is 200×. Scale bar, 100 μm. *MSTN*$^{-/-}$ pigs showed skeletal muscle hypertrophy and significantly increased the muscle fiber area. (**C**) Relative to WT pigs, *MSTN*$^{-/-}$ pigs showed no expression of MSTN, downregulate phosphorylation of Smad2/3 and MyHC IIa, and upregulate MyHC IIb and MyoD in longissimus dorsi (Mus). (**D**) *MSTN*$^{-/-}$ pigs showed increased glycolysis enzymes HK2, PFK1 and PKM2 in longissimus dorsi (Mus). (**E**) The protein expression of MSTN was not detected in intestine (Int) while the α-SMA and Calponin-1 were increased in *MSTN*$^{-/-}$ pigs

compared with the WT pigs. (**F**) Relative expression of tight junction genes *ZO-1* and *Occludin* were enhanced in small intestine of *MSTN*$^{-/-}$ pigs. (**G**) Hematoxylin eosin staining of intestinal morphology. The dotted line indicates the length of the plica and the solid line indicates the thickness of muscularis. Magnification is 40×. Scale bar, 500 μm. *MSTN*$^{-/-}$ pigs showed an increase of muscularis thickness and plica length in small intestine. (**H**) Plots shown were generated using the weighted version of the Unifrac-based PCA. (**I**) Discriminative taxa determined by LEfSe between two groups (log10 LDA>4.8). (**J**) Comparison proportion of genus levels in feces detected by pyrosequencing analysis showed *Treponema*, *Romboutsia*, and *Turicibacter* were increased in *MSTN*$^{-/-}$ pigs. Statistical analysis is performed using Student's *t-test* between WT and *MSTN*$^{-/-}$ pigs. Data are means ± SEM. **p* < 0.05; ***p* < 0.01; ****p* < 0.001; NS, not statistically significant.

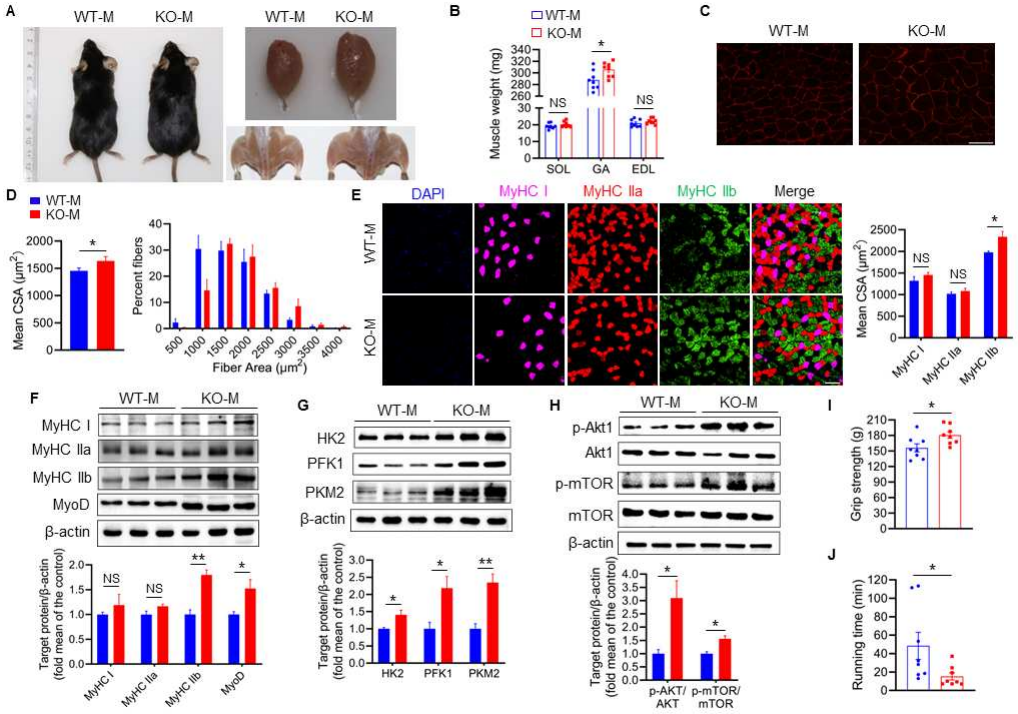

837

838 **Figure 2.** Mice fecal microbiota transplantation from *MSTN* deletion pigs induces type
839 IIb myofiber growth. Mice were treated with porcine fecal microbiota for eight weeks
840 by daily oral gavage after combined antibiotics treatment for a week. WT-M, WT pigs
841 fecal microbiota-received mice (n=8); KO-M, $MSTN^{-/-}$ pigs fecal
842 microbiota-received mice (n=8). (**A**) Representative images of gross appearance and
843 GA of WT-M and KO-M. (**B**) GA mass was increased in KO-M while SOL and EDL
844 were not different between WT-M and KO-M. (**C**) Representative images of GA
845 sections stained with laminin. Magnification is 400×. Scale bar, 50 μm. (**D**)
846 Quantification analysis of myofiber CSA showed that KO-M was larger than WT-M.
847 (**E**) Representative images of GA sections stained with MyHC I (pink), IIa (red), IIb
848 (green) antibodies and nucleuses were stained with DAPI (blue). Magnification is
849 200×. Scale bar, 100 μm. Quantification of myofiber displayed MyHC IIb CSA were
850 increased in KO-M. (**F**) KO-M showed upregulate the level of MyHC IIb and MyoD

in GA. (**G**) The expression of glycolysis enzymes HK2, PFK1 and PKM2 were increased in KO-M GA. (**H**) The Akt/mTOR pathway was activated in KO-M GA. (**I** and **J**) Grip strength was enhanced while running time was reduced in KO-M compared with WT-M. Statistical analysis is performed using Student's *t-test* between WT-M and KO-M groups. Data are means ± SEM. *$p < 0.05$; **$p < 0.01$; NS, not statistically significant.

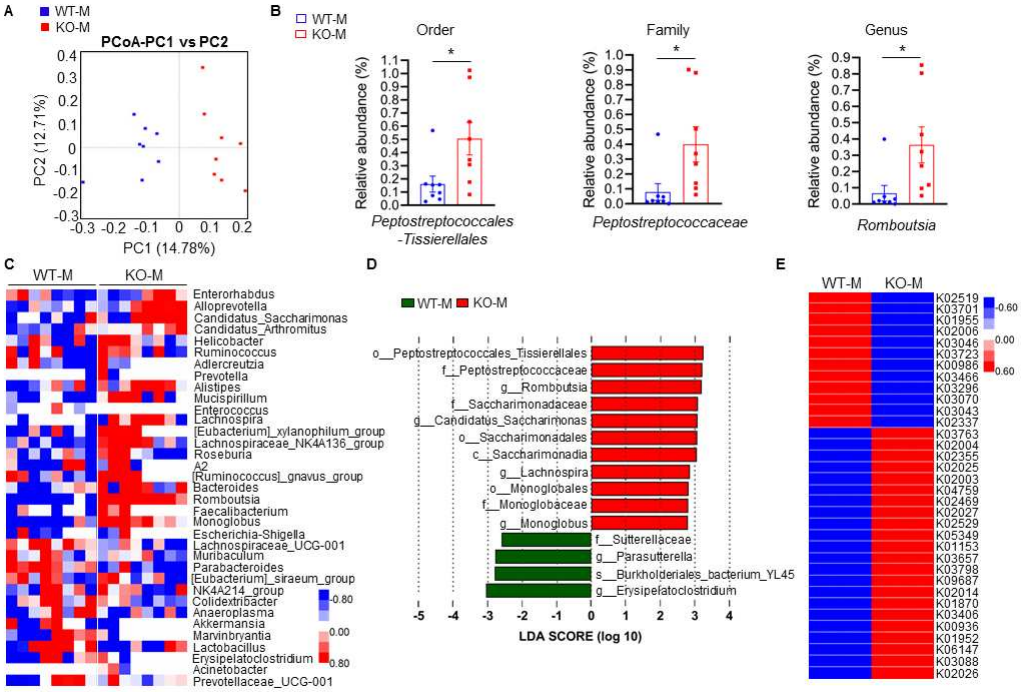

858

859 **Figure 3.** *MSTN*$^{-/-}$ pigs fecal microbiota transplantation alters microbiota composition

860 in mice. Transplanting fecal microbiota of *MSTN*$^{-/-}$ pigs and WT pigs separately to

861 mice (n=8). (**A**) Plots shown were generated using the weighted version of the

862 Unifrac-based PCoA. (**B**) Comparison proportion of order, family and genus levels of

863 *Romboutsia* in feces detected by pyrosequencing analysis. (**C**) Heatmap shows the

864 abundance of top 35 microbial genuses levels was significantly altered by WT and

865 *MSTN*$^{-/-}$ donor pigs between WT-M and KO-M groups. (**D**) Discriminative taxa

866 determined by LEfSe between two groups (log10 LDA>3.5). (**E**) Functional

867 prediction shows that intestinal microbial functions are concentrated in functional

868 pathways related to metabolite synthesis after fecal microbiota transplantation.

869 Statistical analysis is performed using Student's *t-test* between WT-M and KO-M

870 groups. Data are means ± SEM. *$p < 0.05$.

871

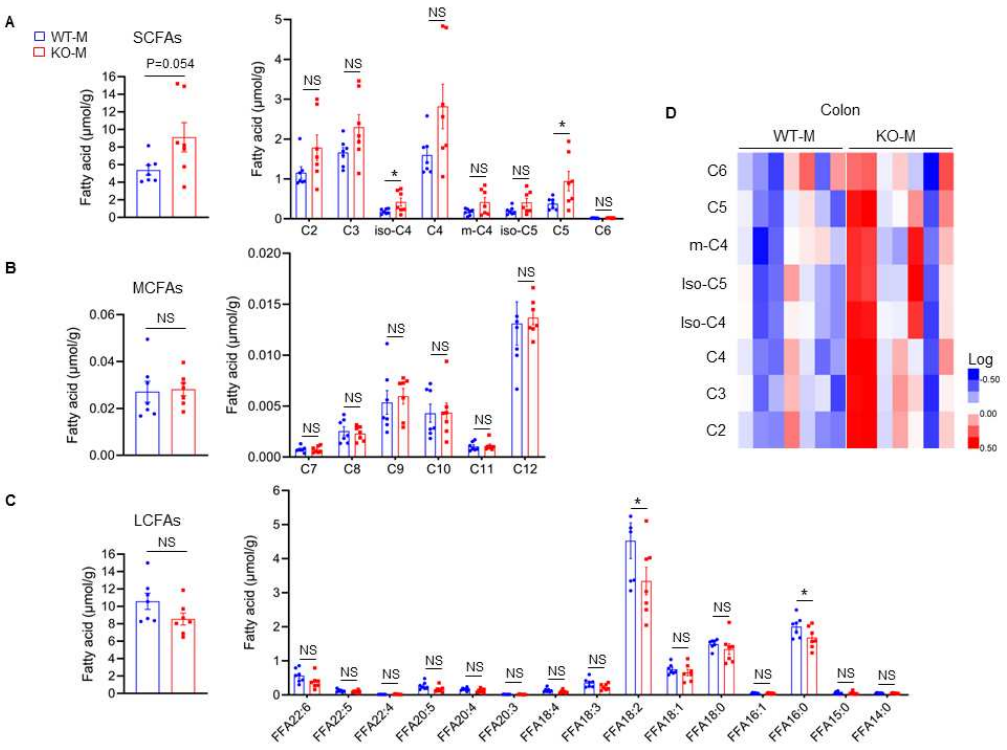

872

873 **Figure 4.** *MSTN*$^{-/-}$ pigs fecal microbiota transplantation alters the level of fatty acids
874 in mice (n=7). (**A**) Fecal microbiota transplantation increased colon total SCFAs
875 (particularly valeric acid and isobutyric acid) in KO-M. (**B**) Fecal microbiota
876 transplantation has no effect on MCFAs between WT-M and KO-M. (**C**) Fecal
877 microbiota transplantation decreased colon FFA18:2 and FFA16:0 of LCFAs in KO-M.
878 (**D**) Heatmap showed the difference of SCFAs between WT-M and KO-M. Statistical
879 analysis is performed using Student's *t-test*. Data are means ± SEM. *$p < 0.05$; NS,
880 not statistically significant.

881

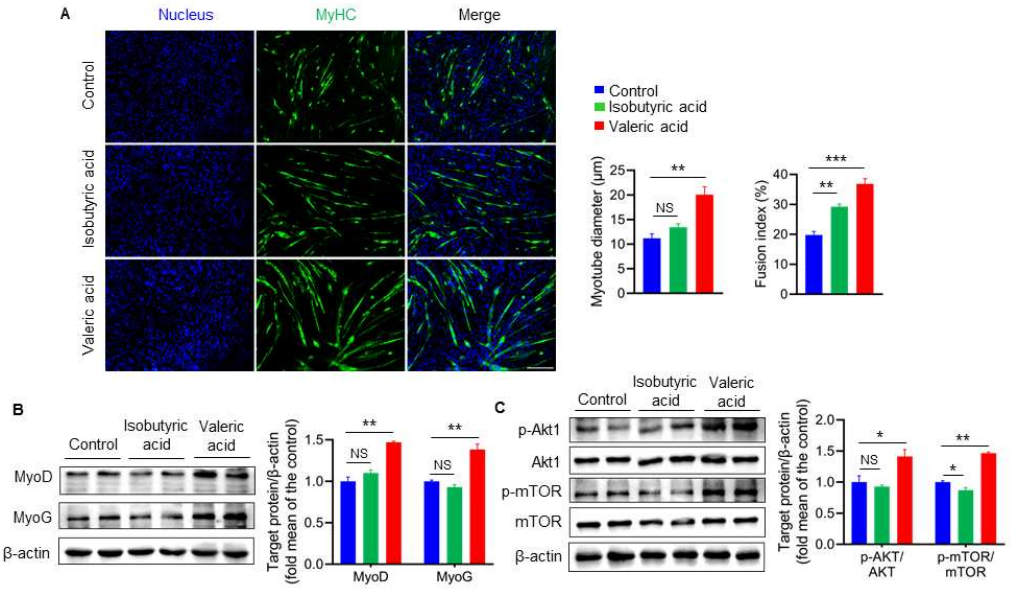

Figure 5. Valeric acid treatment promotes myogenic differentiation of myoblast (n=6). (**A**) Representative images of immunofluorescence stained with a specific antibody to identify MyHC (green) of myotubes and the nucleuses were stained with DAPI (blue). Magnification is 100×. Scale bar, 200 μm. Quantification analysis displayed valeric acid treatment increased the diameter and fusion index of myotube, while isobutyric acid only increased the myotube fusion index. (**B**) Valeric acid treatment increased the expression of MyoD and MyoG in C2C12 myoblasts. (**C**) Valeric acid treatment activated the Akt/mTOR pathway. Statistical analysis is performed using one-way ANOVA. Data are means ± SEM. *$p < 0.05$; **$p < 0.01$; ***$p < 0.001$; NS, not statistically significant.

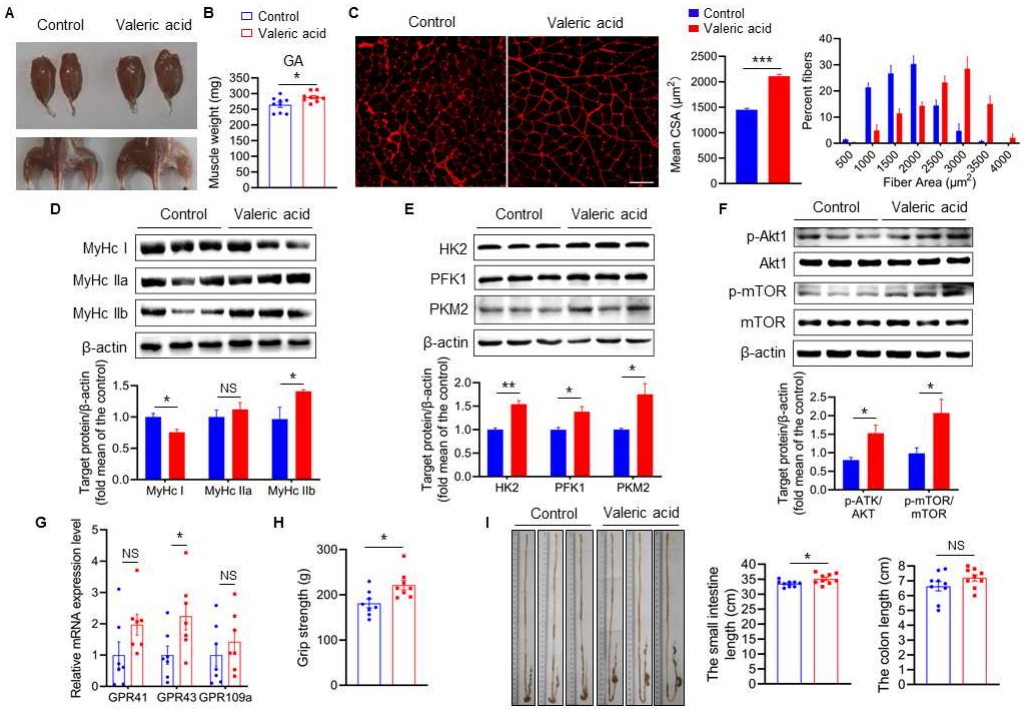

894

895 **Figure 6.** Valeric acid induced type IIb myofiber growth and increased GA mass in
896 mice. Mice were treated with valeric acid (100 mg/kg) for five weeks by daily oral
897 gavage (n=8-9). (**A**) Representative images of gross appearance and GA of control
898 and valeric acid treated mice. (**B**) Valeric acid treatment increased GA mass. (**C**)
899 Representative images of GA sections stained with laminin, showed valeric acid
900 treatment increased CSA of myofiber. Magnification is 200×. Scale bar, 100 μm.
901 Western blot analysis showed that valeric acid treatment increased the levels of (**D**)
902 MyHC IIb, (**E**) glycolysis enzymes HK2, PFK1 and PKM2, and (**F**) activated the
903 Akt/mTOR pathway in GA compared with control mice. (**G**) Real-time PCR analysis
904 indicated that valeric acid treatment enhanced relative mRNA expression of SCFAs
905 receptor *GPR43* in GA. (**H**) Valeric acid treatment improved grip strength. (**I**)
906 Representative images of cecum, small intestine, and colon of mice, showed valeric
907 acid treatment inceresed small intestine length. Statistical analysis is performed using

908 Student's *t-test*. Data are means ± SEM. *$p < 0.05$; **$p < 0.01$; ***$p < 0.001$; NS, not

909 statistically significant.

910

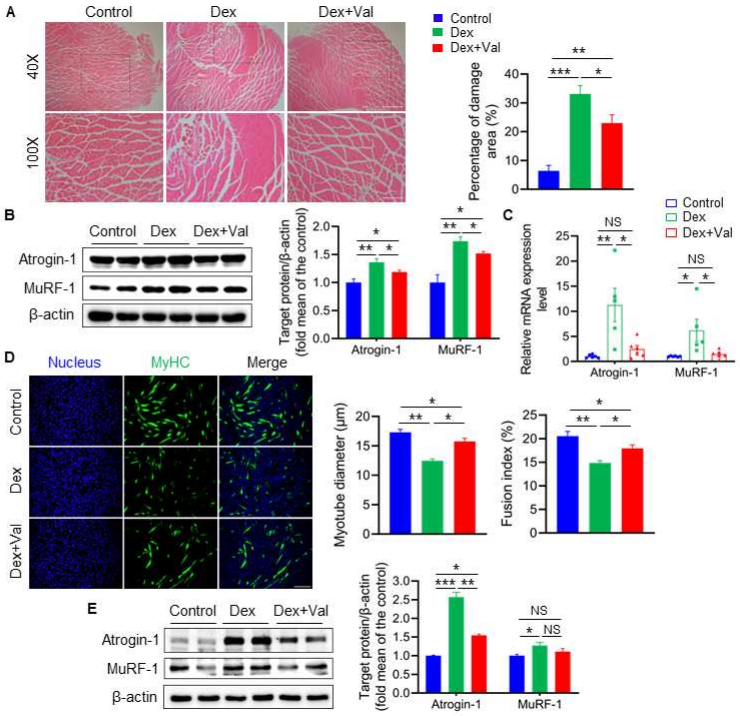

Figure 7. Valeric acid ameliorates Dex-induced skeletal muscle and myotube atrophy. Mice were treated with intraperitoneal injection of 20 mg/kg Dex every 2 day for two weeks and 100 mg/kg of valeric acid was fed orally every day before two weeks of Dex injection (n=5). Myotube atrophy was induced with 100 μM/L of Dex, and 5 mM/L of valeric acid was supplied at the same time (n=6). (**A**) Hematoxylin eosin staining of GA morphology. Magnification is 40×. Scale bar, 500 μm. Quantification analysis showed that Dex induced the myofiber damage, and valeric acid treatment decreased the percentage of damage area. (**B**) Western blot analysis showed that Dex induced the expression of Atrogin-1 and MuRF-1 in GA, while valeric acid treatment reduced the level of these. (**C**) Real-time PCR analysis of relative expression of atrophy genes (*Atrogin-1* and *MuRF-1*) in GA, showed valeric acid treatment could inhibit the expression of these genes induced by Dex. (**D**) Immunofluorescence stained with a specific antibody was used to identify MyHC (green) of myotube and

the nucleus were stained with DAPI (blue). Magnification is 100×. Scale bar, 200 μm. Quantification analysis showed valeric acid treatment could improve the reduction of myotubes diameter and fusion index induced by Dex. (**E**) Western blot analysis showed valeric acid treatment could inhibit the expression of Atrogin-1 induced by Dex in C2C12 myotubes and had no effect on MuRF-1 induced by Dex. Statistical analysis is performed using one-way ANOVA with *Least Significant Difference test*. Data are expressed as means ± SEM. *$p < 0.05$; **$p < 0.01$; ***$p < 0.001$; NS, not statistically significant.

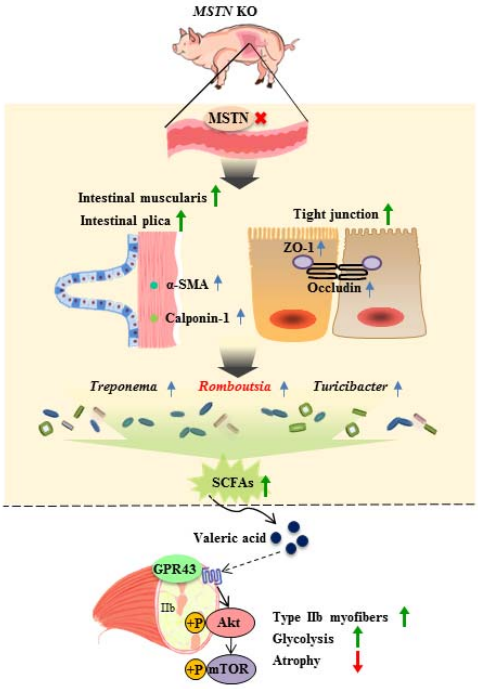

Figure 8. Schematic illustration. Intestine MSTN deficiency altered the intestinal structure, reshaped gut microbiota, and gut microbiota metabolite-valeric acid can activate Akt/mTOR pathway through GPR43 to stimulate fast-twitch glycolytic skeletal muscle growth.

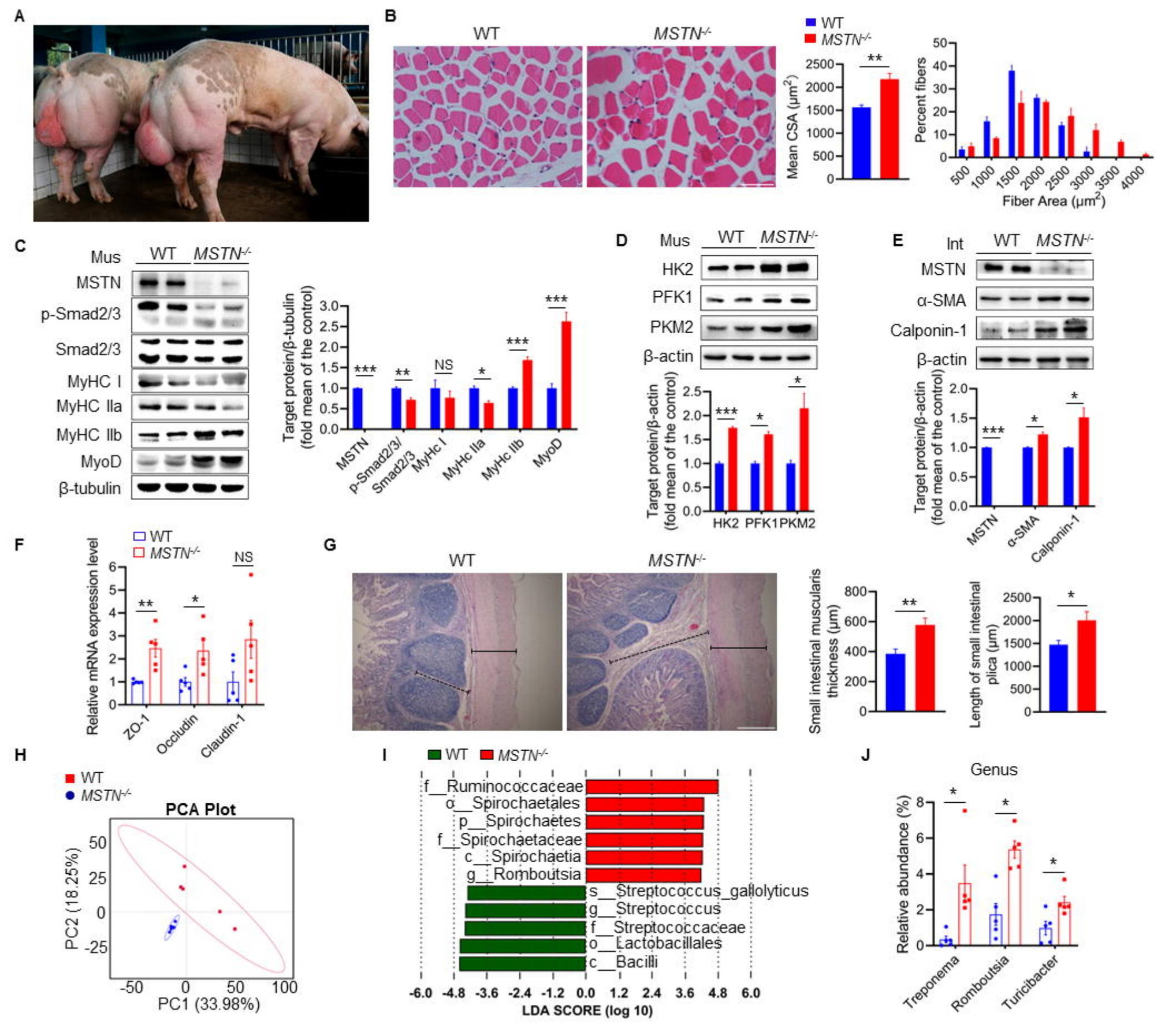
A
B
WT
MSTN-/-
Mean CSA (μm2)
Percent fibers
Fiber Area (μm2)
C
Mus
MSTN
p-Smad2/3
Smad2/3
MyHC I
MyHC IIa
MyHC IIb
MyoD
β-tubulin
Target protein/β-tubulin (fold mean of the control)
D
HK2
PFK1
PKM2
β-actin
Target protein/β-actin (fold mean of the control)
E
Int
α-SMA
Calponin-1
F
Relative mRNA expression level
ZO-1
Occludin
Claudin-1
G
Small intestinal muscularis thickness (μm)
Length of small intestinal plica (μm)
H
PCA Plot
PC1 (33.98%)
PC2 (18.25%)
I
f__Ruminococcaceae
o__Spirochaetales
p__Spirochaetes
f__Spirochaetaceae
c__Spirochaetia
g__Romboutsia
s__Streptococcus_gallolyticus
g__Streptococcus
f__Streptococcaceae
o__Lactobacillales
c__Bacilli
LDA SCORE (log 10)
J
Genus
Relative abundance (%)
Treponema
Romboutsia
Turicibacter

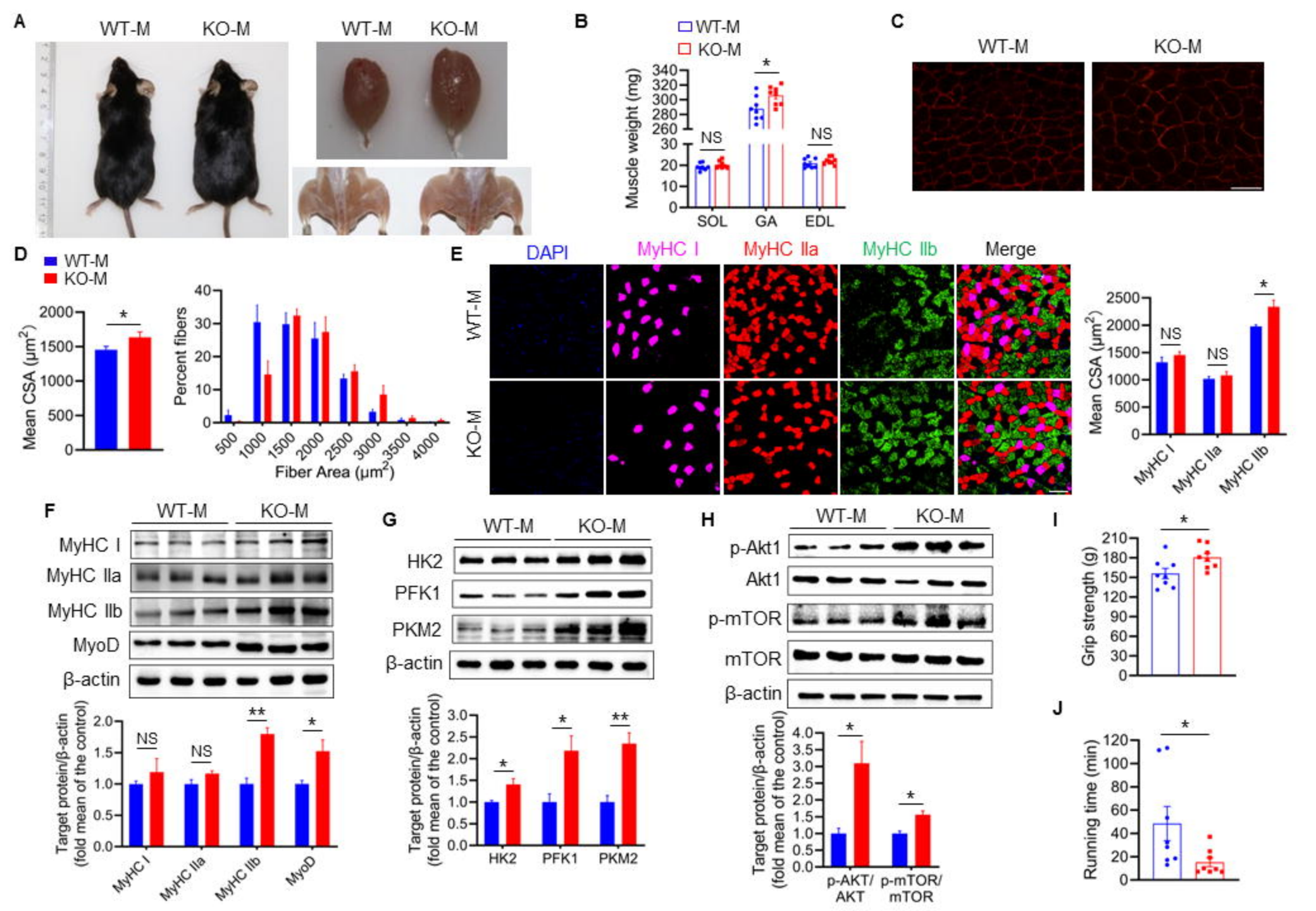
A
WT-M
KO-M
WT-M
KO-M
B
WT-M
KO-M
Muscle weight (mg)
340
320
300
280
260
30
20
10
0
NS
*
NS
SOL
GA
EDL
C
WT-M
KO-M
D
WT-M
KO-M
Mean CSA (μm²)
2000
1500
1000
500
0
*
Percent fibers
40
30
20
10
0
500
1000
1500
2000
2500
3000
3500
4000
Fiber Area (μm²)
E
DAPI
MyHC I
MyHC IIa
MyHC IIb
Merge
WT-M
KO-M
Mean CSA (μm²)
2500
2000
1500
1000
500
0
NS
NS
*
MyHC I
MyHC IIa
MyHC IIb
F
WT-M
KO-M
MyHC I
MyHC IIa
MyHC IIb
MyoD
β-actin
Target protein/β-actin (fold mean of the control)
2.0
1.5
1.0
0.5
0.0
NS
NS
**
*
MyHC I
MyHC IIa
MyHC IIb
MyoD
G
WT-M
KO-M
HK2
PFK1
PKM2
β-actin
Target protein/β-actin (fold mean of the control)
3.0
2.5
2.0
1.5
1.0
0.5
0.0
*
*
**
HK2
PFK1
PKM2
H
WT-M
KO-M
p-Akt1
Akt1
p-mTOR
mTOR
β-actin
Target protein/β-actin (fold mean of the control)
4.0
3.5
3.0
2.5
2.0
1.5
1.0
0.5
0.0
*
*
p-AKT/ AKT
p-mTOR/ mTOR
I
Grip strength (g)
210
180
150
120
90
60
30
0
*
J
Running time (min)
120
100
80
60
40
20
0
*

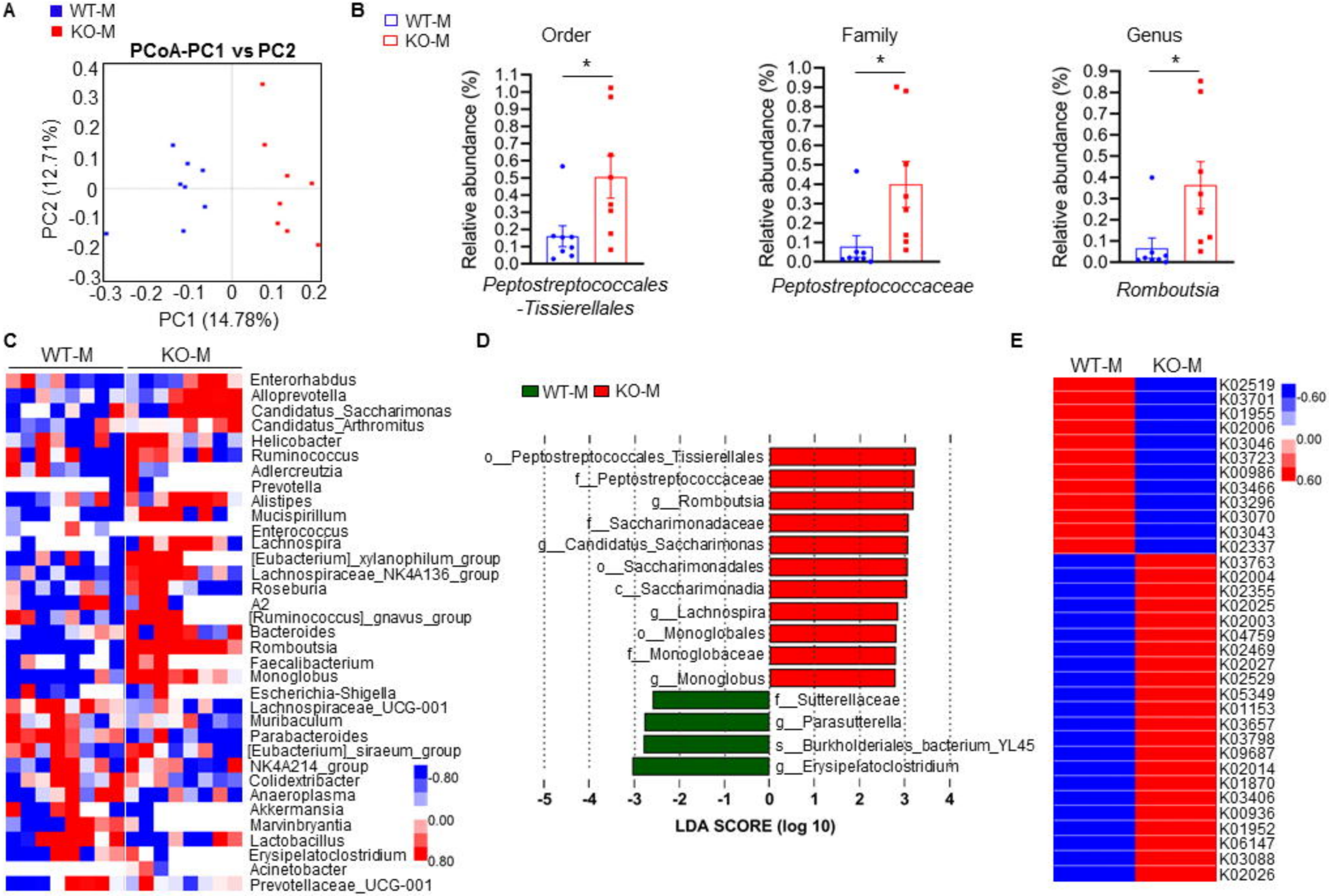
A
WT-M
KO-M
PCoA-PC1 vs PC2
PC2 (12.71%)
PC1 (14.78%)
B
WT-M
KO-M
Order
Family
Genus
Relative abundance (%)
Peptostreptococcales -Tissierellales
Peptostreptococcaceae
Romboutsia
C
WT-M
KO-M
Enterorhabdus
Alloprevotella
Candidatus_Saccharimonas
Candidatus_Arthromitus
Helicobacter
Ruminococcus
Adlercreutzia
Prevotella
Alistipes
Mucispirillum
Enterococcus
Lachnospira
[Eubacterium]_xylanophilum_group
Lachnospiraceae_NK4A136_group
Roseburia
A2
[Ruminococcus]_gnavus_group
Bacteroides
Romboutsia
Faecalibacterium
Monoglobus
Escherichia-Shigella
Lachnospiraceae_UCG-001
Muribaculum
Parabacteroides
[Eubacterium]_siraeum_group
NK4A214_group
Colidextribacter
Anaeroplasma
Akkermansia
Marvinbryantia
Lactobacillus
Erysipelatoclostridium
Acinetobacter
Prevotellaceae_UCG-001
-0.80
0.00
0.80
D
WT-M
KO-M
o__Peptostreptococcales_Tissierellales
f__Peptostreptococcaceae
g__Romboutsia
f__Saccharimonadaceae
g__Candidatus_Saccharimonas
o__Saccharimonadales
c__Saccharimonadia
g__Lachnospira
o__Monoglobales
f__Monoglobaceae
g__Monoglobus
f__Sutterellaceae
g__Parasutterella
s__Burkholderiales_bacterium_YL45
g__Erysipelatoclostridium
LDA SCORE (log 10)
E
WT-M
KO-M
K02519
K03701
K01955
K02006
K03046
K03723
K00986
K03466
K03296
K03070
K03043
K02337
K03763
K02004
K02355
K02025
K02003
K04759
K02469
K02027
K02529
K05349
K01153
K03657
K03798
K09687
K02014
K01870
K03406
K00936
K01952
K06147
K03088
K02026
-0.60
0.00
0.60

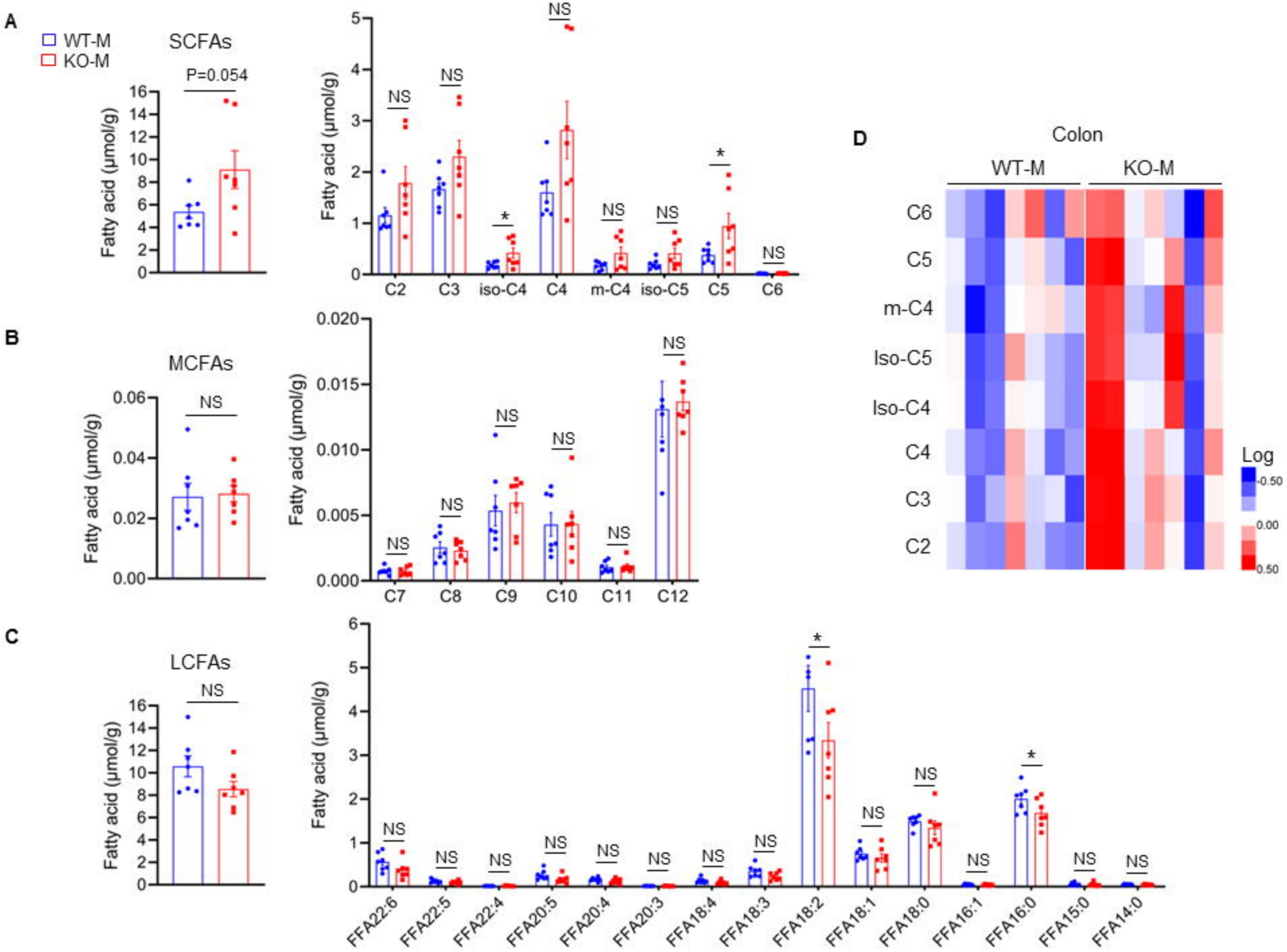
A
WT-M
KO-M
SCFAs
P=0.054
Fatty acid (μmol/g)
NS
*
C2
C3
iso-C4
C4
m-C4
iso-C5
C5
C6
B
MCFAs
C7
C8
C9
C10
C11
C12
C
LCFAs
FFA22:6
FFA22:5
FFA22:4
FFA20:5
FFA20:4
FFA20:3
FFA18:4
FFA18:3
FFA18:2
FFA18:1
FFA18:0
FFA16:1
FFA16:0
FFA15:0
FFA14:0
D
Colon
WT-M
KO-M
C6
C5
m-C4
Iso-C5
Iso-C4
C4
C3
C2
Log
0.50
0.00
0.50

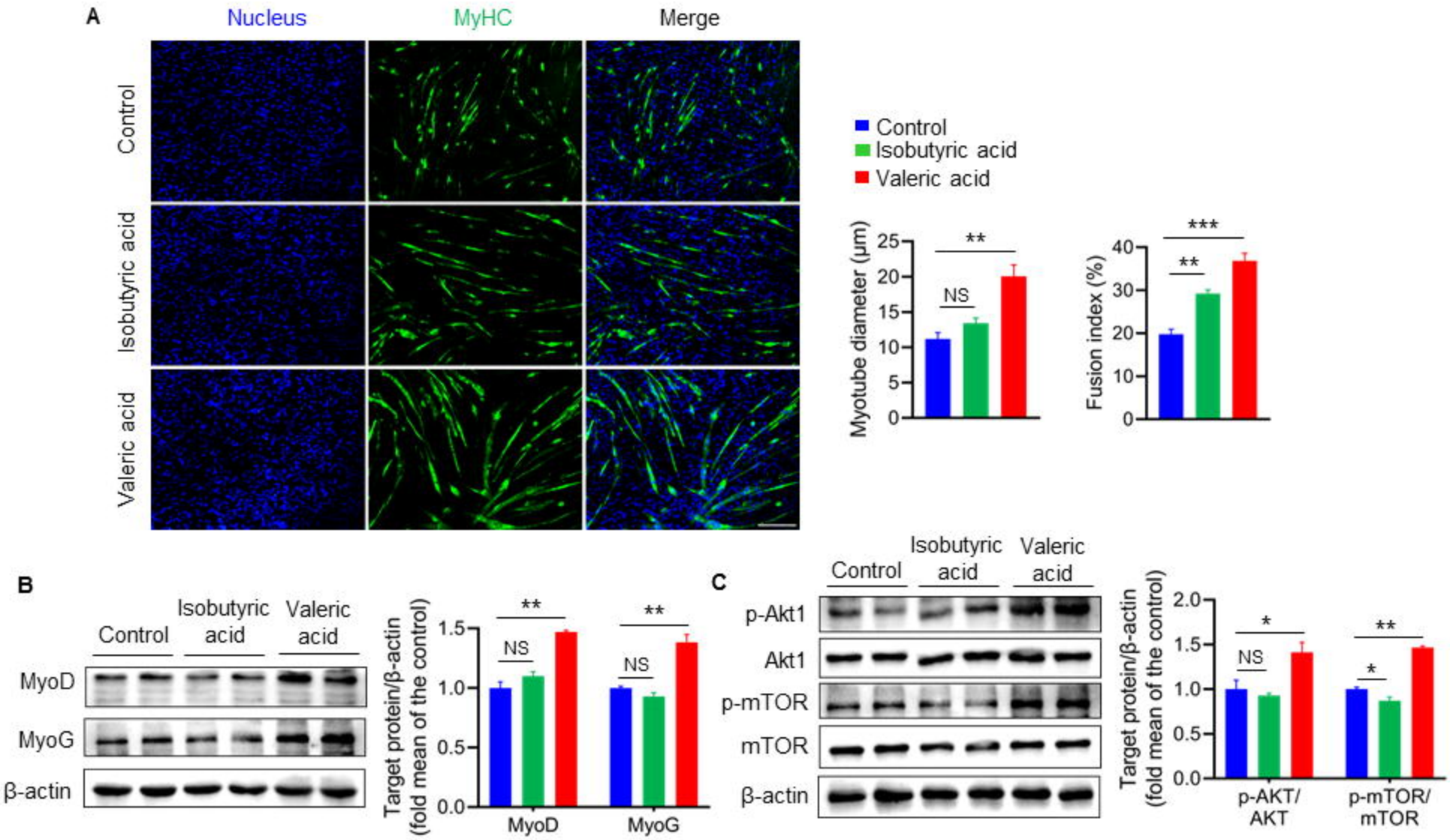
A
Nucleus
MyHC
Merge
Control
Isobutyric acid
Valeric acid
Control
Isobutyric acid
Valeric acid
Myotube diameter (μm)
Fusion index (%)
NS
**
***
B
Control
Isobutyric acid
Valeric acid
MyoD
MyoG
β-actin
Target protein/β-actin (fold mean of the control)
C
p-Akt1
Akt1
p-mTOR
mTOR
β-actin
p-AKT/ AKT
p-mTOR/ mTOR
*

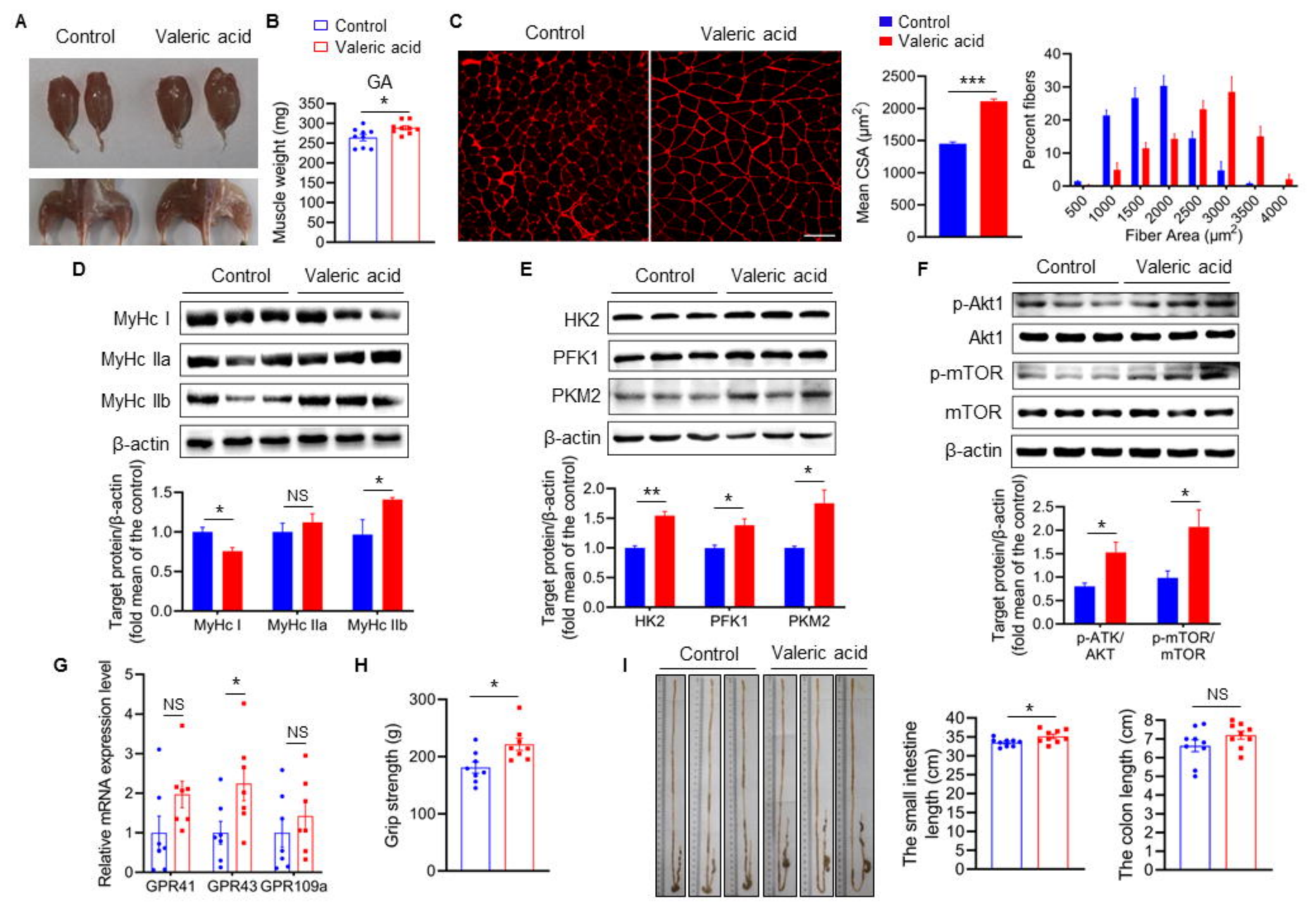
A
Control
Valeric acid
B
Control
Valeric acid
GA
Muscle weight (mg)
C
Control
Valeric acid
Mean CSA (μm²)
Percent fibers
Fiber Area (μm²)
D
Control
Valeric acid
MyHc I
MyHc IIa
MyHc IIb
β-actin
Target protein/β-actin (fold mean of the control)
E
HK2
PFK1
PKM2
F
p-Akt1
Akt1
p-mTOR
mTOR
p-ATK/AKT
p-mTOR/mTOR
G
Relative mRNA expression level
GPR41
GPR43
GPR109a
H
Grip strength (g)
I
The small intestine length (cm)
The colon length (cm)

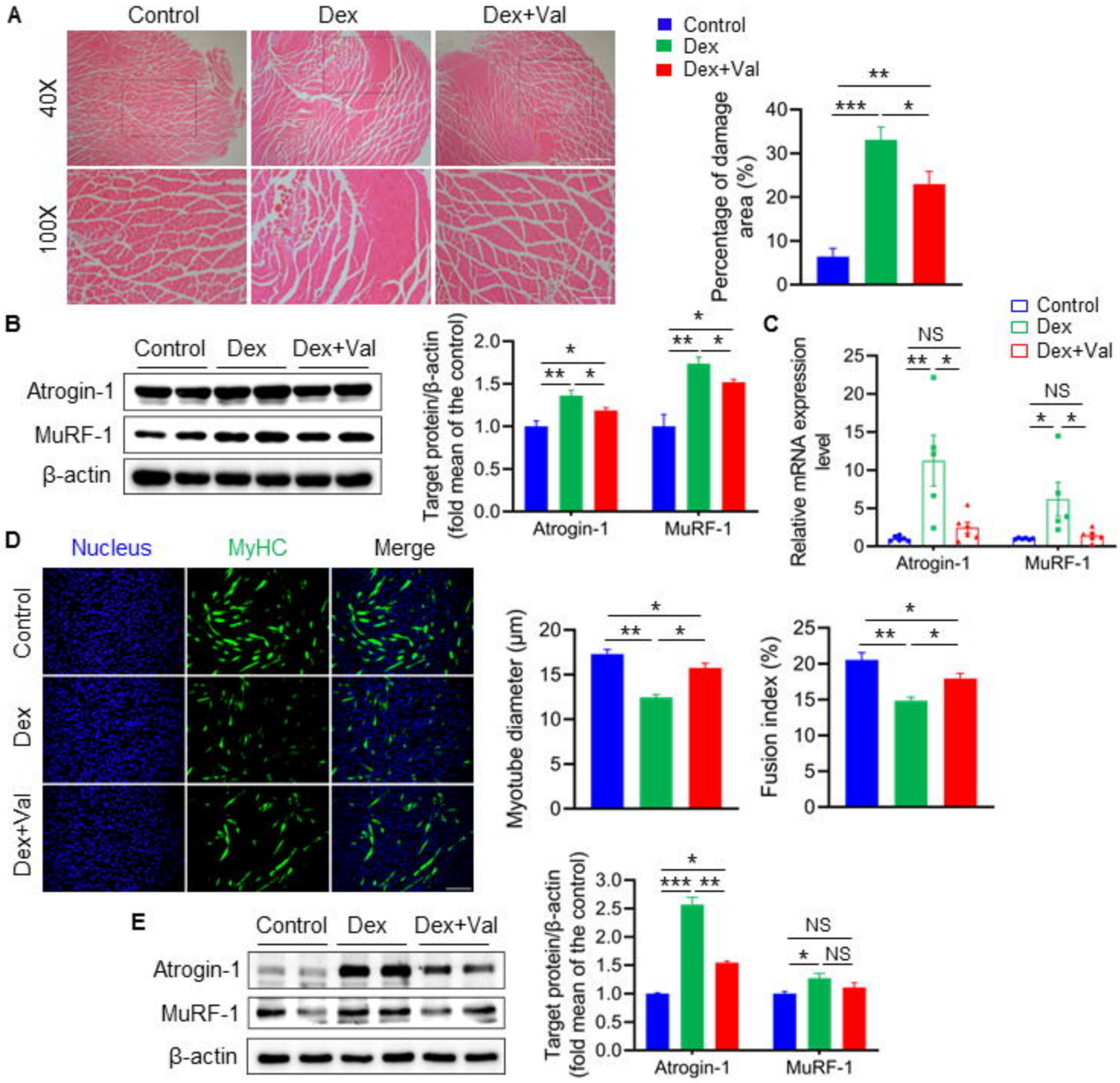
A
Control
Dex
Dex+Val
40X
100X
Control
Dex
Dex+Val
Percentage of damage area (%)
B
Control
Dex
Dex+Val
Atrogin-1
MuRF-1
β-actin
Target protein/β-actin (fold mean of the control)
Atrogin-1
MuRF-1
C
Control
Dex
Dex+Val
Relative mRNA expression level
NS
Atrogin-1
MuRF-1
D
Nucleus
MyHC
Merge
Control
Dex
Dex+Val
Myotube diameter (μm)
Fusion index (%)
E
Control
Dex
Dex+Val
Atrogin-1
MuRF-1
β-actin
Target protein/β-actin (fold mean of the control)
NS
Atrogin-1
MuRF-1

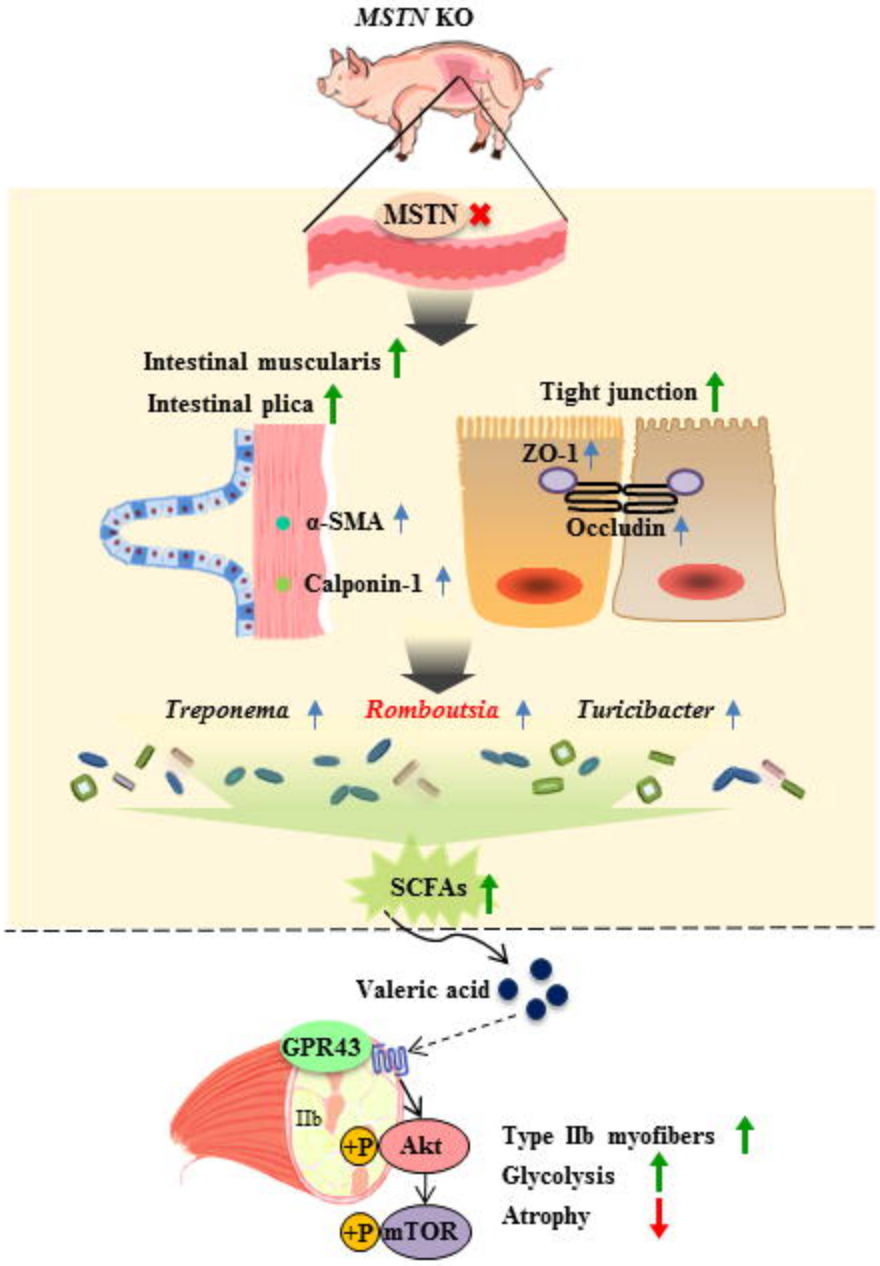
MSTN KO
MSTN
Intestinal muscularis
Intestinal plica
α-SMA
Calponin-1
Tight junction
ZO-1
Occludin
Treponema
Romboutsia
Turicibacter
SCFAs
Valeric acid
GPR43
IIb
+P
Akt
+P
mTOR
Type IIb myofibers
Glycolysis
Atrophy